Rivers, J., Varghese, L., Yousif, R., Whitaker, F., Skeat, S., & Al-Shaikh, I. (2019). The Geochemistry of Qatar Coastal Waters and Its Impact on Carbonate Sediment Chemistry and Early Marine Diagenesis. *Journal of Sedimentary Research*, *89*(4), 293-309. https://doi.org/10.2110/jsr.2019.17

Journal of Sedimentary Research

Journal of Sedimentary Research, 2019, v. 89, 293–309
Research Article
DOI: http://dx.doi.org/10.2110/jsr.2019.17

THE GEOCHEMISTRY OF QATAR COASTAL WATERS AND ITS IMPACT ON CARBONATE SEDIMENT CHEMISTRY AND EARLY MARINE DIAGENESIS

JOHN M. RIVERS,[1] LINSO VARGHESE,[1] RUQAIYA YOUSIF,[1] FIONA F. WHITAKER,[2] SABRINA L. SKEAT,[1] AND ISMAIL AL-SHAIKH[1]
[1]*ExxonMobil Research Qatar, Science and Technology Park, Tech 2, Doha, Qatar*
[2]*University of Bristol, School of Earth Sciences, Office G30, Wills Memorial Building, Queens Road, Clifton BS8 1RJ, U.K.*
e-mail: John.m.rivers@exxonmobil.com

ABSTRACT: **The southern margin of the Arabian Gulf is a "classic" shallow-water, evaporative, carbonate-producing setting. The sediments and early diagenetic products creating the "Great Pearl Bank" of the United Arab Emirates to the east and accumulating in the coastal regions of Qatar to the west have long been studied as modern analogs for ancient evaporitic carbonate deposits of the rock record. An integrated study measuring the chemistry of Qatar subtidal coastal waters, evaporating tidal-pond waters (to halite saturation), and meteoric pond waters was undertaken encompassing both the dry (fall) and wet (winter/spring) seasons of 2016–2017. Measured parameters included temperature, pH, dissolved oxygen, and alkalinity, as well as major-ion (Na^+, Ca^{2+}, Mg^{2+}, K^+, Sr^{2+}, Cl^-, and SO_4^{2-}) and stable-isotope ($\delta^{18}O$ and δD) composition. Initial concentration by evaporation (to $\sim$ 90 practical salinity units (psu)) is interpreted to drive minor diagenetic aragonite precipitation. Further evaporation initially causes minor aragonite dissolution followed by gypsum and halite precipitation. One pond showed evidence of ongoing replacive dolomitization interpreted to be driven by H_2S formation and oxidation in association with microbial breakdown of organic matter. The stable-isotope composition of water in restricted ponds is a function of the degree of evaporation and dilution by meteoric waters during the wet season. Unexpectedly, beyond 350 psu, $\delta^{18}O$ and δD continue to rise reaching values greater than 12 and 60‰, respectively. The slope of the $\delta^{18}O$–δD regression line exhibits no differences between dry and wet seasons.**

During collection of coastal waters (up to $\sim$ 90 psu), live *Pirenella cingulata* (previously *Cerithidea cingulata*) gastropods were collected and their shells analyzed for $\delta^{18}O$ and $\delta^{13}C$, as well as Sr^{2+} and Ca^{2+} concentration. The $\delta^{18}O$ of water and *Pirenella* from the same sample site exhibits a strong correlation ($R^2 \geq 0.85$) with a slope of $\sim$ 1, suggesting that the shells may be a useful chemical archive for the isotopic composition of past oceans. The $\delta^{18}O$ and $\delta^{13}C$ of the shells correlate positively, likely reflecting greater sequestration of ^{12}C into organic matter in more restrictive evaporative settings. The intercept of the $\delta^{18}O$ and $\delta^{13}C$ correlation shifts between dry and wet seasons, and is interpreted to reflect average seawater temperature differences during recent growth. There is also a strong correlation ($R^2 \geq 0.85$) between shell $\delta^{18}O$ and measured water salinity, reflecting their mutual control by degree of evaporation. The Sr^{2+} content of the gastropods does not correlate well with any measured oceanographic parameter, or show evidence of systematic seasonal change.

INTRODUCTION

The Arabian Gulf is a relatively shallow (mostly $<$ 60 m) marine embayment that represents the foreland basin of the Zagros Mountains to the north (Fig. 1). The southern margin of the Arabian Gulf, with water depths of less than 20 m, is a site of extensive carbonate sedimentation (Kinsman 1964; Purser 1973; Purser and Seibold 1973; Wagner and van der Togt 1973; Alsharan and Kendall 2003; Wilkinson and Drummond 2004). This depositional setting includes the "Trucial Coast" of northern Oman and the United Arab Emirates, which hosts the "Great Pearl Bank," and is considered an important modern example of a homoclinal carbonate-ramp setting (Read 1982). In the western part of this evaporative warm-water domain, the coastal waters of Qatar host photozoan carbonate deposits (Purser and Evans 1973; Shinn 1973; Billeaud et al 2014; Purkis et al 2017) that include localized ooid bodies (Loreau and Purser 1973).

Studies of early carbonate diagenesis in this setting are numerous and generally focus on marine cementation (Shinn 1969; Evamy 1973; Purser and Loreau 1973), as well as diagenetic overprint in the supratidal sabkha setting (Evans et al. 1969; Butler et al 1982). Particular focus has been given to early dolomitization of marine carbonate deposits in sabkha settings, and the geochemistry of associated pore waters (Illing et al. 1965; Hsu and Schneider 1973; Illing and Taylor 1993; Bontognali et al. 2010; Sadooni et al. 2010; Brauchli et al. 2016). Whereas it is widely recognized that the open seawater in the region is subject to evaporation, there has been little prior study of associated geochemical changes. The motivation behind this contribution is to understand how the chemistry of seawater evolves during evaporation, and how that evolution impacts the chemistry of the carbonate deposits and their early diagenesis.

Published Online: April 2019
 1527-1404/19/089-293

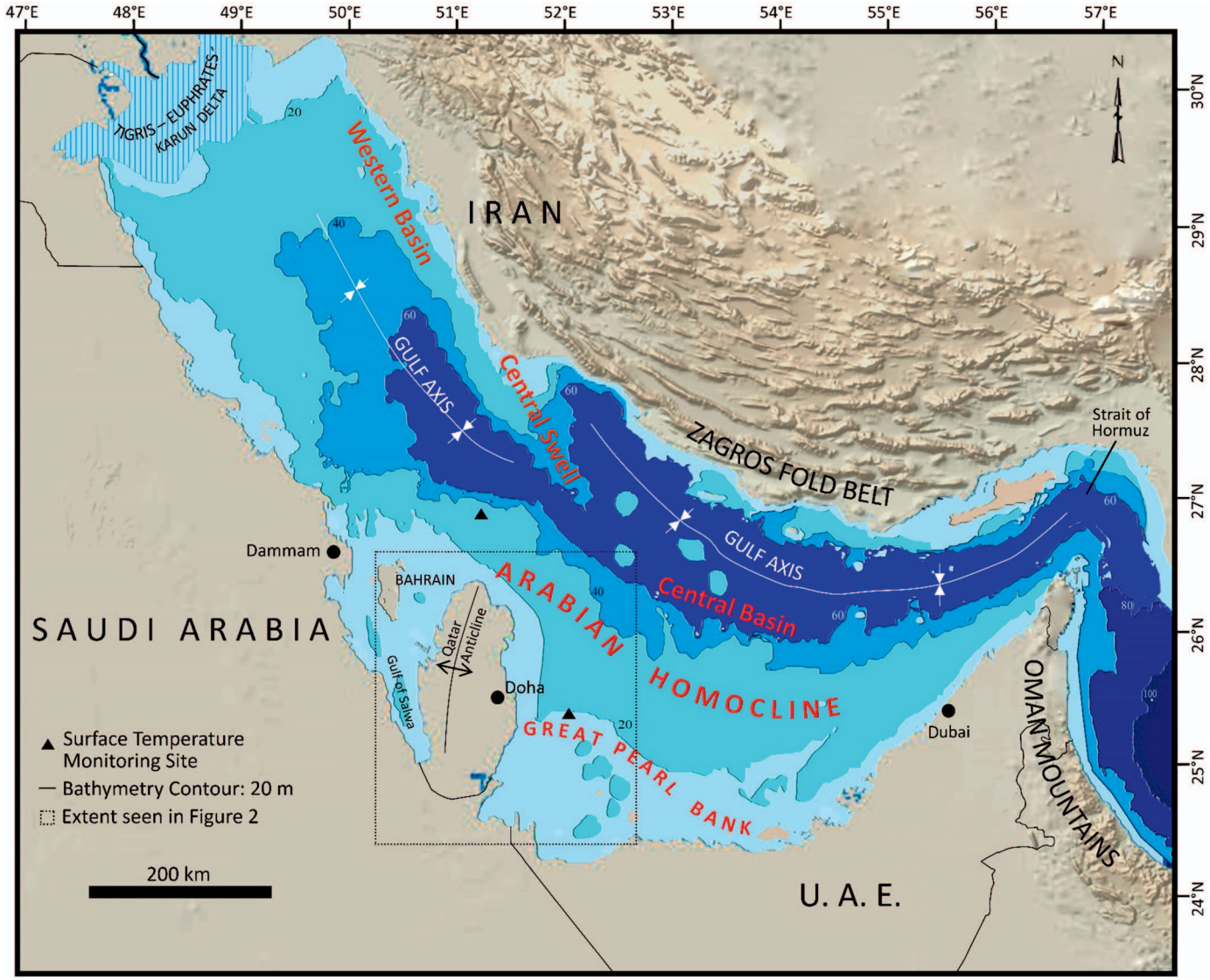

FIG. 1.—Map of Arabian Gulf showing bathymetry (based on Azam et al. 2006; Elshorbagy et al. 2007; Al-Ansari et al. 2015; Elhakeem et al. 2015) and geographic location of the study area. Location of open gulf water-temperature monitoring stations is also shown (triangles). The area shown in Figure 2 is boxed.

GEOLOGICAL AND GEOGRAPHICAL SETTING

The sovereign state of Qatar forms a peninsula of approximately 190 km length (north–south) and 90 km width that protrudes northward into the Arabian Gulf from the Kingdom of Saudi Arabia (Fig. 1). It forms part of an active plate margin where the underlying Arabian plate is colliding with the Eurasian plate, resulting in the uplift of the Zagros mountain range northward in Iran (Stern and Johnson 2010), and the formation of a foreland basin.

Surface rocks of Qatar are predominantly limestones and dolostones of Eocene age (Dammam and Rus fms.), with Miocene (Dam Fm.), and Pliocene (Hofuf Fm.) rocks cropping out only in the southwestern area of the country (Seltrust 1980). The coastal areas are rimmed with Quaternary deposits including Pleistocene and Holocene carbonate rocks and sediments, as well as clastic (quartz-rich) eolian sands. Common peritidal environments include sabkhas and tidal flats, with near-shore open subtidal sediments being grainy and mollusk-rich (Wagner and van der Togt 1973; Purser and Evans 1973). The northern (windward) coastline hosts a barrier-island system, fronted by a moribund coral reef (Purkis et al. 2017). Coral reefs are also found forming isolated banks along the eastern Qatar coastline (Purser and Evans 1973), where ooid deposits have been identified (Loreau and Purser 1973). Southeastern Qatar hosts the evaporative Inland Sea channel and lagoon system (Fig. 2), where intertidal flats are the site of robust microbial-mat formation (Paulo and Dittrich 2013). Subtidal waters in this restricted system at times reach gypsum saturation (Purser 1973).

CLIMATE AND OCEANOGRAPHY

The Arabian Gulf is a subtropical epicontinental sea that lies within the global arid belt, ~ 25° north of the equator (Fig. 1). The basin has an area of 250,000 sq. km, is shallow (mostly < 60 meters water depth) and semi-restricted. This large embayment is affected by "Shamal winds" from the north and elevated summer air temperatures (frequently attaining 50°C), leading to evaporation and concentration of marine waters. Open Gulf waters commonly reach salinities of 40 practical salinity units (psu) or higher (Kampf and Sadrinasab 2006), and exceed 70 psu in lagoons (Purser and Seibold 1973). Surface water temperatures typically range

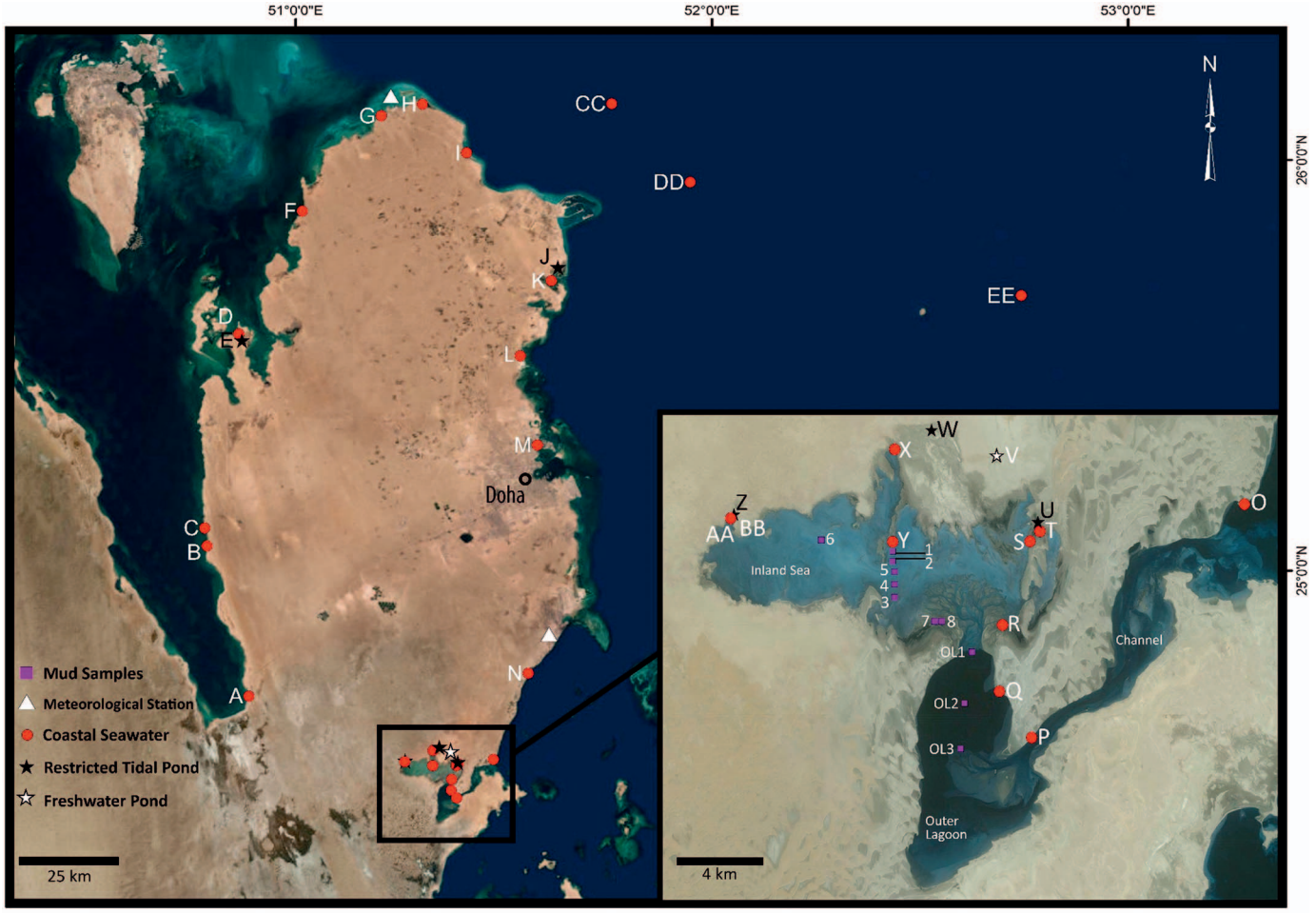

FIG. 2.—Map of Qatar showing location of water-sample sites and meteorological stations referred to in the text. Inset: The Inland Sea channel and lagoon system. The Inland Sea is less than 2 meters water depth and is separated by a channel 1 km wide and 3 m deep from the outer lagoon, where water depths reach 18 m. This connects with the open gulf via a 12 km channel that is less than ~ 7 m deep. Base map: WorldView-2 satellite data acquired in November 2011 by DigitalGlobe Inc.

between 20 and 30°C during the year (Kampf and Sadrinasab 2006) although fluctuations in lagoons can range from 15 to 40°C (Purser and Seibold 1973).

Circulation models by Kampf and Sadrinasab (2006) suggest that surface water enters the Arabian Gulf at the Strait of Hormuz and flows in a cyclonic (anticlockwise) pattern, moving northwestward along the Iranian coastline before rotating at the northern end of the Gulf and flowing southeastward into the Gulf of Salwa and along the UAE coastline. During the summer these shallow southern surface waters are concentrated through evaporation, reaching modeled salinities of > 45 psu. The concentrated waters cool during the winter and outflow through the Strait of Hormuz as bottom-hugging density-driven currents.

METHODS

Surface waters from three distinct settings were sampled for this study (Supplemental Table S1). *Coastal waters* were mostly sampled within 10 m of the shoreline in the very shallow subtidal settings by wading. Three samples (OG1a, OG2a, and OG3a) were taken offshore east and northeast of Qatar (see Supplemental Table S1 and Fig. 2). *Restricted-marine tidal ponds* were sampled on shore. These ponds are only episodically flooded by marine waters during some spring tides, or by fresh waters after significant rains. Between flooding events, the ponds commonly evaporate to gypsum or halite saturation. Following a winter rain event, one *freshwater retention pond* was sampled at two different times after significant evaporation had taken place. Additionally, at water-sampling stations where *Pirenella cingulata*, previously classified as *Cerithidea cingulata* (Reid and Ozawa 2016), gastropods were observed, live specimens were collected for chemical analyses. Modern aragonitic mud was also collected from the inland sea for isotopic analyses. Finally, data on 2016–2017 marine water temperature, as well as data on air temperature, wind speed, wind direction, and humidity were requested from and provided by the Qatar Civil Aviation Authority (Department of Meteorology) (Fig. 3) for sites marked in Figures 1 and 2.

In Situ Water Measurements

During the fall of 2016, at the end of the dry season, coastal (n = 23) and restricted tidal pond (n = 3) waters were measured in the field for temperature (± 0.01°C), salinity (± 0.1 psu), dissolved oxygen (± 0.01 mg/l or 0.1%), and pH (± 0.01 pH units). With the exception of sample GS-4a, all field measurements were made using a Yellow Springs Instrument (YSI) EXO Water Quality Monitoring Platform. For samples with salinity > 70 psu as measured in the field, salinity was re-measured in the laboratory after dilution using a HACH HQ 440d multimeter. Coastal (n = 20), tidal pond (n = 13), and freshwater pond (n = 2) waters were measured for the same parameters during the winter/spring of 2016–2017 after significant rainfall had occurred. Some pond waters were sampled

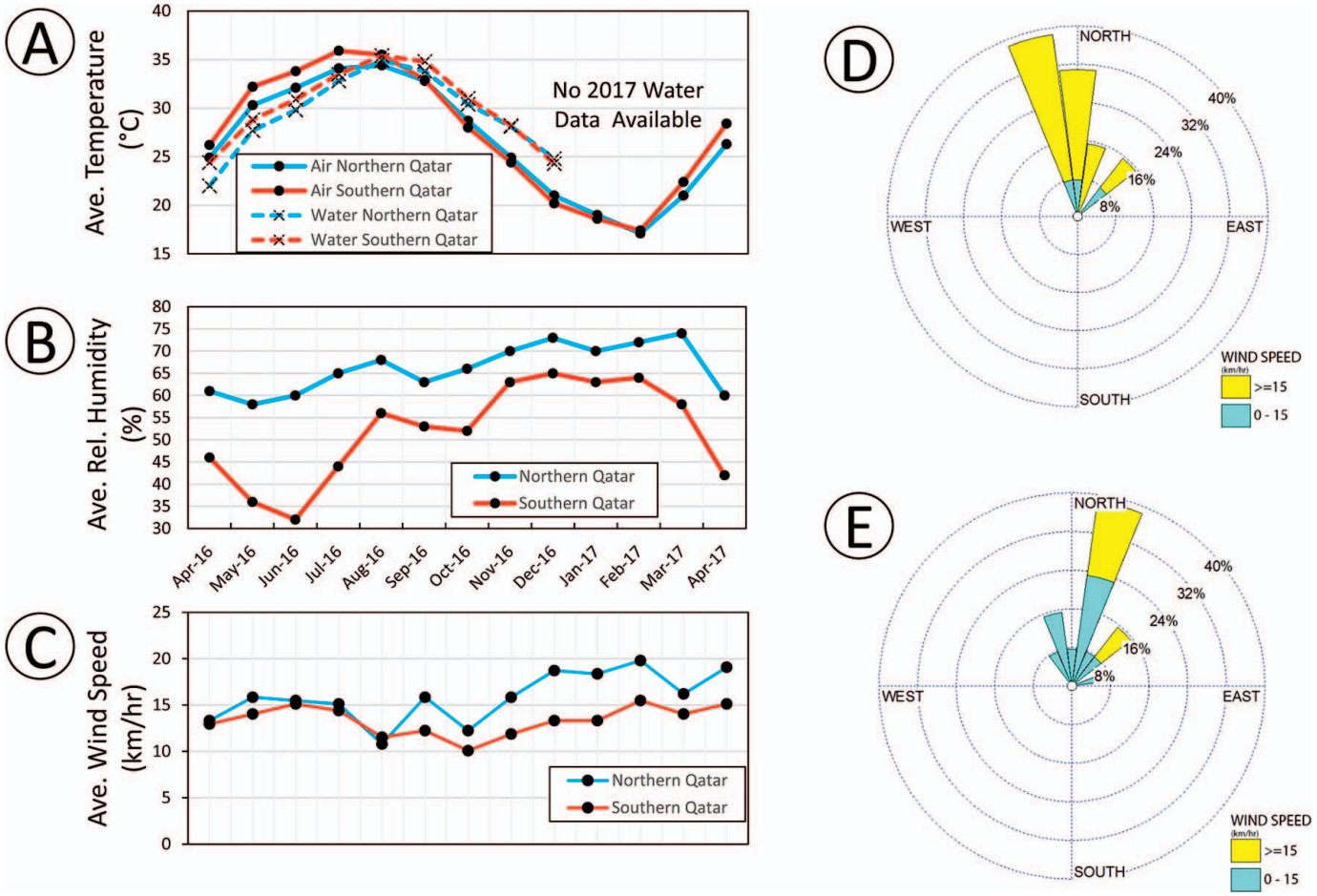

FIG. 3.—**A)** Average monthly air-temperature data from northern and southern Qatar meteorological stations (location shown in Fig. 2) and average monthly sea-surface water temperature from monitoring stations located off northern and southern Qatar (location shown in Fig. 1). Only 2016 water-temperature data are available. **B)** Average monthly humidity from northern and southern Qatar meteorological stations. **C)** Average monthly wind speed from northern and southern Qatar meteorological stations. **D)** Wind rose showing average monthly direction during this study from the northern Qatar meteorological station (Fig. 2). **E)** Wind rose showing average monthly direction during this study from the southern Qatar meteorological station (Fig. 2).

several times throughout the year to document their chemical variability and evolution. Measurements if *in-situ* temperature (± 0.1°C), salinity (± 0.1 psu), and pH (± 0.01 pH units) were made for sample GS-4a using a Hach HQ30d sensor.

Laboratory Water Measurements

During *in situ* measurements of water chemistry, a suite of water samples were taken for laboratory measurements of $\delta^{18}O$ and δD (n = 54), alkalinity (n = 24), and major/minor ion content including Na^{+}, Ca^{2+}, Mg^{2+}, and Sr^{2+} (n = 53), as well as SO_4^{2-} and Cl^{-} (n = 19) (Supplemental Table S1). Water samples taken for $\delta^{18}O$ and δD measurement were passed through an 0.45 µm filter at collection site during transfer to vials that were filled to capacity and sealed such that no head space remained. Waters were analyzed at the Center for Stable Isotope Biogeochemistry (CSIB), University of California, Berkeley. $\delta^{18}O_{water}$ were analyzed by continuous flow (CF) using a Thermo Gas Bench II interfaced to a Thermo Delta Plus XL mass spectrometer. The method described in the Thermo Gas Bench II operating manual, ThermoQuest, Oct 1999 was used. In brief, 20–200 µL of water (depending on the sample volume available) for both standards and samples were pipetted into 10 mL glass vials and quickly sealed. The vials were then purged with 0.2% CO_2 in helium and allowed to equilibrate at room temperature for at least 48 hours. The $\delta^{18}O$ in the CO_2 was then analyzed. Long-term external precision is better than ± 0.12‰. δD in water was analyzed in dual inlet (DI) using a hot chromium reactor unit (H/Device™) interfaced with a Thermo Delta Plus XL mass spectrometer. Long-term external precision is ± 0.80‰.

Bicarbonate alkalinity was measured by titration with measurement precision of 0.97% based on external standards. Chloride measurements were made by argentometric titration with 0.39% precision, and sulfate was measured by turbidimetric method with precision of 2.1%. For cations, water samples (100 ml) were filtered through a 0.45 µm filter paper on site, and the liquid was then acidified (2% v/v) with nitric acid of trace-metal-grade. The acidified samples were then analyzed for Na^{+}, Ca^{2+}, Mg^{2+}, K^{+}, and Sr^{2+} using a Varian 730ES Inductively Coupled Plasma Optical-Emission Spectrometer (ICP-OES). The analytical precision based on n = 4 for Na^{+} is 1.9%, K^{+} is 1.8%, Ca^{2+} is 1.6%, Mg^{++} is 1.4%, and Sr^{2+} is 0.4%. All spike and quality control standards recoveries were within the range of ± 10% of the true value. The ion balance error for all samples with a full suite of major ions (n = 20) was +1.4 ± 1.5.

The thermodynamic modeling package PHREEQC 3.0 (Parkhurst and Appello 2013) was used to calculate the distribution and activities of all aqueous species, the partial pressure of CO_2, and saturation states (log IAP/K) of aragonite, calcite, dolomite, and gypsum, using the Pitzer database

TABLE 1.— *Sample names, location, as well as isotopic and trace-element data from gastropods collected (live) during water sampling. $\delta^{18}O$ and salinity measured for seawater at the time of gastropod collection are displayed for reference.*

Fall Gastropod Measurements								
Sample Name	**Map Location**	**$\delta^{13}C$ (‰ VPDB)**	**$\delta^{18}O$ (‰ VPDB)**	**Ca^{2+} Wt%**	**Sr^{2+} (ppm)**	**Sr^{2+} (Ca-Norm X 1000)**	**$\delta^{18}O_{Sw}$ (‰ VSMOW)**	**Seawater Salinity (psu)**
ISWS-1a	BB	2.8	4.0	42	850.2	2.0	7.0	81.9
ISWS-1a	BB	3.3	4.1	24	535.4	2.2	7.0	81.9
ISWS-1a	BB	2.7	4.2	42	944.7	2.3	7.0	81.9
ISWS-2a	X	3.6	4.5	40	1020.8	2.5	7.5	87.4
ISWS-2a	X	3.3	4.3				7.5	87.4
ISWS-3a	R	3.2	2.4	41	1279.0	3.1	5.3	62.4
ISWS-3a	R	3.6	2.1				5.3	62.4
ISWS-4a	S	2.9	3.5	42	1257.5	3.0		84.8
GS-1a	A	1.9	1.6	44	1130.1	2.6	4.6	57.3
GS-1a	A	2.7	2.3	39	1209.4	3.1	4.6	57.3
GS-2a	B	3.9	2.4	43	1214.6	2.8	4.6	56.3
GS-2a	B	1.5	1.8	38	1233.7	3.2	4.6	56.3
GS-4a	D	2.2	0.7	45	1085.3	2.4	3.4	47.0
GS-4a	D	1.8	0.8	41	925.6	2.3	3.4	47.0
GS-5a	F	1.4	0.2	41	1127.0	2.7	3.2	49.1
Fu-1a	I	1.3	-1.3				1.6	40.7
KCh-3a	O	2.0	0.8	42	947.8	2.3		46.6
KCh-3a	O	2.7	1.1	38	1233.7	3.2		46.6
AT-2a	K	0.6	-0.7					41.5
Winter/Spring Gastropod Measurements								
Sample Name	**Map Location**	**$\delta^{13}C$ (‰ VPDB)**	**$\delta^{18}O$ (‰ VPDB)**	**Ca^{2+} Wt%**	**Sr^{2+} (ppm)**	**Sr^{2+}(Ca-Norm X 1000)**	**$\delta^{18}O_{Sw}$ (‰ VSMOW)**	**Seawater Salinity (psu)**
ISWS-6a	AA	3.5	5.3	42	824.1	1.9		73.1
ISWS-4b	S	3.8	4.2				4.6	64.7
Sh-1b	G	2.1	1.0	35	816.4	2.3	2.6	43.3
AR-1b	H	-1.0	1.4	42	908.6	2.2	2.8	42.0
Si-1a	L	2.8	1.2	36	1293.1	3.6	2.7	41.8
GS-1b	A	2.2	2.4				4.6	55.8
GS-3b	C	1.9	2.9	35	914.9	2.6	4.6	55.3
GS-4b	D	4.0	1.9	36	1276.3	3.6	3.0	46.2
ISWS-6b	AA	3.8	5.1	41	1223.0	3.0	5.9	65.6
GS-5b	F	0.0	1.0	35	956.4	2.7	2.9	45.3
Dolo 2a	Y	3.4	3.4	40	1038.1	2.6	5.4	60.0
ISWS-4c	S	3.5	3.5	41	1335.5	3.2	6.4	70.8
AT-2b	K	1.3	0.0	41	1027.5	2.5	2.6	44.1

(Plummer et al. 1988) which takes into account specific ion interactions that occur in high-ionic-strength solutions (Krumgalz 2001). Uncertainties in saturation index (SI) and PCO_2 values are estimated as 0.02 log units (0.04 log units for dolomite) and 21 ppm respectively and are dominated by uncertainty in pH.

Chemical Measurements of Gastropods and Aragonitic Mud

At all sampling stations where gastropods were observed (n = 24), living specimens were recovered for both stable-isotope and trace element analysis (Table 1). Separately, aragonitic mud samples (n = 8) were collected from the Inland Sea channel and lagoon system. As with the water samples, isotopic measurements were performed at the Center for Stable Isotope Biogeochemistry (CSIB), University of California, Berkeley. Gastropod shells and aragonitic mud were cleaned with an ethanol solution, before being dried and ground with an agate mortar and pestle to a fine powder. 10–100 μg of powdered carbonate was used for both carbon and oxygen isotope analyses. Several replicates of one international standard NBS19, and two lab standards ($CaCO_3$-I and II) were measured along with samples for each run. The overall external analytical precision is about +0.05‰ for $\delta^{13}C$ and about +0.07‰ for $\delta^{18}O$. Carbon and oxygen isotopic compositions are reported in standard δ notation ($\delta^{13}C$ and $\delta^{18}O$) in units of per mil relative to Vienna Peedee Belemnite (VPDB) standard.

For cations, ground shell splits from isotopic analyses (0.05–0.1 g) were digested in trace-metal-grade nitric acid. The acidified samples were then analyzed for Ca^{2+} and Sr^{2+} using a Varian 730ES inductively coupled plasma optical emission spectrometer (ICP-OES). The analytical precision for Ca^{2+} is 1.6% and for Sr^{2+} is 0.4%. All spike and quality-control standards recoveries were within the range of ± 10% of the true value.

RESULTS

Air and Water Temperature, Humidity, and Wind Data (2016–2017)

Average monthly air temperatures at coastal meteorological stations in northern and southern Qatar (Fig. 2) ranged from a maximum of 36°C in summer to a minimum of 17°C in winter (Fig. 3A). Water temperatures at two locations in the open Arabian Gulf waters (see Fig. 1) followed air temperatures, with a lag time of approximately one month (data for 2017 not available), and ranged between 35°C and 22°C. Whereas latitudinal air-

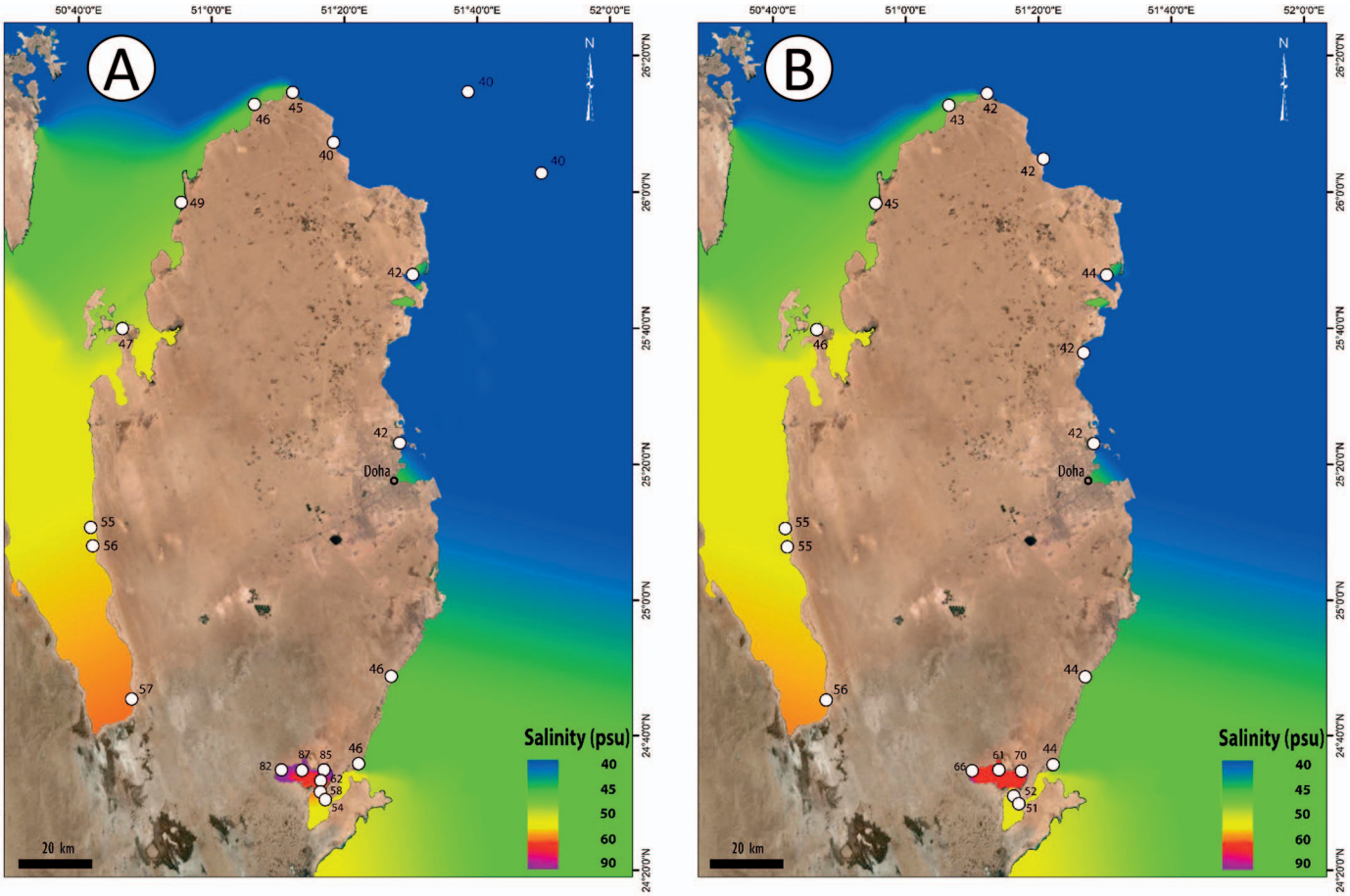

FIG. 4.—Map of surface water salinity in **A)** fall, **B)** winter and spring. This map was generated using field sampling (2016 and 2017) at sites around the Qatari coast (white dots), and integration of contour trends from literature (Erftemeijer et al. 2004; Sadrinasab and Kenarkohi 2009; Rezaei-Latifi 2016). Basemap: GeoEye satellite data captured in 2011 by DigitalGlobe, Inc (Esri).

temperature differences were minimal in the fall and winter, air temperatures in the spring and summer were higher by an average of 2°C at southern stations than those in the north.

Relative humidity at the northern station was consistently > 60%, reaching almost 75% during winter months (Fig. 3C). Humidity in southern Qatar was considerably lower and showed higher seasonal variability, with a minimum of 30% in summer, and a maximum of 65% in winter when stronger winds brought humid air from the Gulf onshore. Long-term records show that rainfall totals are generally higher in the north of the country (Al Mamoon et al. 2014). According to of the Qatar Meteorology Department of the Civil Aviation Authority, rainfall was negligible during the months of April through October 2016, whereas several significant country-wide rain events occurred between November 2016 and March of 2017 (no quantitative data for publication).

For most of the study period Qatar was affected by the "shamal" winds from the north (Fig. 3C–E). Mean monthly wind speeds range from 12 to 20 km/h at the northern station, compared to 10–15 km/h at the southern station. Wind speed was generally higher in winter and spring (Fig. 3C).

Water Chemistry

Coastal seawaters and waters from restricted tidal ponds that flood only on spring tides or after major rain events were sampled in the fall (September–November) of 2016 after an extended period of aridity over the summer, as well as during the winter and spring months (December–May) of 2016–2017 after significant rain events and before the onset of elevated summer temperatures. One evaporating freshwater retention pond (perched water following rain) was also sampled during the latter period, but only after weeks of initial evaporation.

***In situ* Measurements (Temperature, Salinity, pH, and Dissolved Oxygen).**—Temperatures of coastal and restricted marine pond samples taken from September to November of 2016 vary between 25° and 35°C, with all measurements prior to November greater than 28°C (Supplemental Table S1), consistent with data on open-marine-water temperature (Fig. 3A). In winter coastal temperatures dip to 20–22°C, and increase in spring to 25–33°C (Supplemental Table S1), with most samples measuring between 25°C and 32°C (temperatures of open-marine surface water are not available for this time interval). Some temperature measurements from restricted ponds in this period are higher (up to 26°C in winter), and most spring samples are 35–37°C.

Measured fall and winter/spring surface seawater salinities are broadly similar with the exception of the Inland Sea (Supplemental Table S1; Fig. 4A, B). Open gulf waters northeast of Qatar have salinities in the 40–42 psu range (fall measurements only), whereas in the Gulf of Salwa to the west of Qatar salinities are between 50 and 60 psu. Salinities of the Inland Sea exceed 85 psu in the summer and are generally less than 70 psu in the winter/spring. Measured salinities of waters from restricted tidal ponds vary from ~ 70 to 340 psu, or halite saturation (Supplemental Table S1).

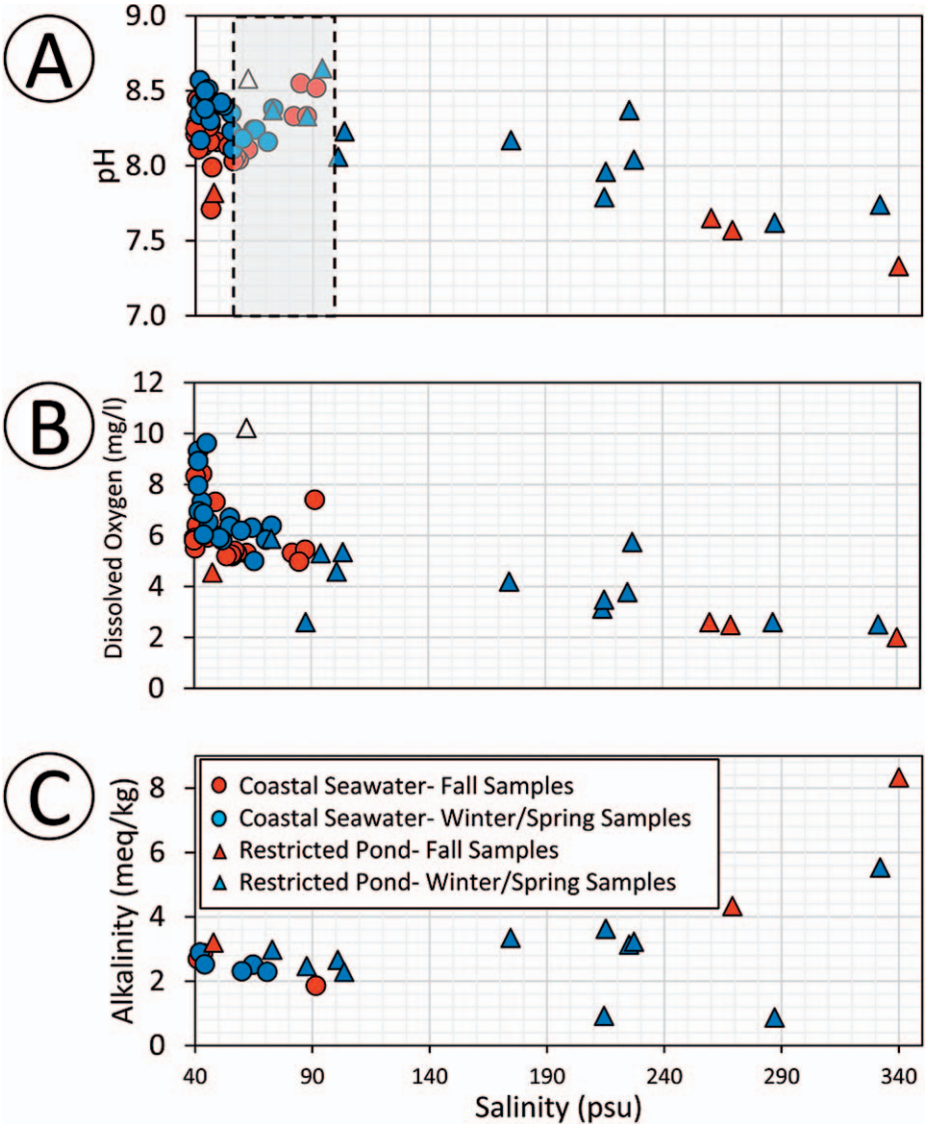

FIG. 5.—Trends in **A)** pH, **B)** dissolved oxygen, and **C)** alkalinity with varying salinity for fall and winter/spring water samples. White triangle represents a sample from a restricted pond at the edge of a mangrove biome (site J, Fig. 2). All other ponds in this study were unvegetated, and the anomalously high DO and pH levels in this sample are likely the result of mangrove photosynthesis. Shaded box highlights increasing pH with salinity between 60 and 100 psu.

As expected, ephemeral surface retention ponds exhibit salinities less than 0.5 psu, even after considerable evaporation (Supplemental Table S1).

Measurements of coastal-seawater pH mostly vary between 8.0 and 8.6, with a higher pH in winter/spring (8.35 ± 0.23) than in the fall (8.19 ± 0.42) (Supplemental Table S1). The pH of tidal-pond waters is highly variable, ranging from 7.3 to 8.6, but there is too little data from the fall to evaluate seasonality. The pH varies systematically with salinity (Fig. 5A). Coastal water samples show a reduction in pH with salinity up to ~ 60 psu, but this trend appears to reverse as salinity increases to ~ 100 psu (boxed area in Fig. 5A). One exception to this trend was from a mangrove pond where a high pH (8.6) was measured. Restricted tidal ponds show that at higher salinities, pH decreases with increasing salinity, with an order-of-magnitude increase in acidity from ~ 100 psu to halite saturation. The two measurements from an evaporating freshwater retention pond have pH values of ~ 8.8 (Supplemental Table S1).

The measured dissolved oxygen (DO) of coastal waters with salinities less than ~ 45 psu is variable, ranging from 5 to 10 mg/l with a mean of 7.2 ± 1.3 (Fig. 5B). With increasing salinity, seawater DO falls below 7 mg/l for almost all measurements. DO measurements of restricted-tidal-pond waters are predominantly less than 6 mg/l, generally decreasing with increasing salinity to ~ 2 mg/l. DO levels in the freshwater pond were ~ 9 mg/l (Supplemental Table S1). As with pH, DO of water from the mangrove pond was anomalously high (> 10 mg/l) and off the trend.

Major Ion Composition.—Alkalinity of both seawater and tidal-pond water of less than ~ 50 psu salinity is ~ 3 meq/kg, decreasing with increasing salinity to ~ 2 meq/kg at ~ 100 psu (Supplemental Table S1, Fig. 5C). The limited number of samples of lower-salinity restricted tidal-pond waters show an alkalinity of 0.6 meq/kg higher than in coastal waters of comparable salinity. In general, the alkalinity of more saline tidal pond waters increases with salinity, exceeding 8 meq/kg as evaporation drives waters toward halite saturation (~ 350 psu). Exceptions include the alkalinities of two tidal pond samples, ISSF-1a and ISSF-1b, which were both collected in December two weeks apart, and measure ~ 1 meq/kg.

The variation of Na^+, Cl^-, SO_4^{2-}, Sr^{2+}, and K^+ with salinity are shown in Figures 6 and 7A. Na^+ and Cl^- concentrations increase linearly with salinity from ~ 13 g/l and ~ 25 g/l, respectively at 40 psu, to ~ 110 g/l and ~ 160 g/l at 280 psu (Fig. 6A, B). At greater salinities Na^+ begins to decease toward ~ 90 g/l, whereas Cl^- increases to ~ 190 g/l. SO_4^{2-} generally increases over the same salinity range from ~ 3 g/l to ~ 32 g/l

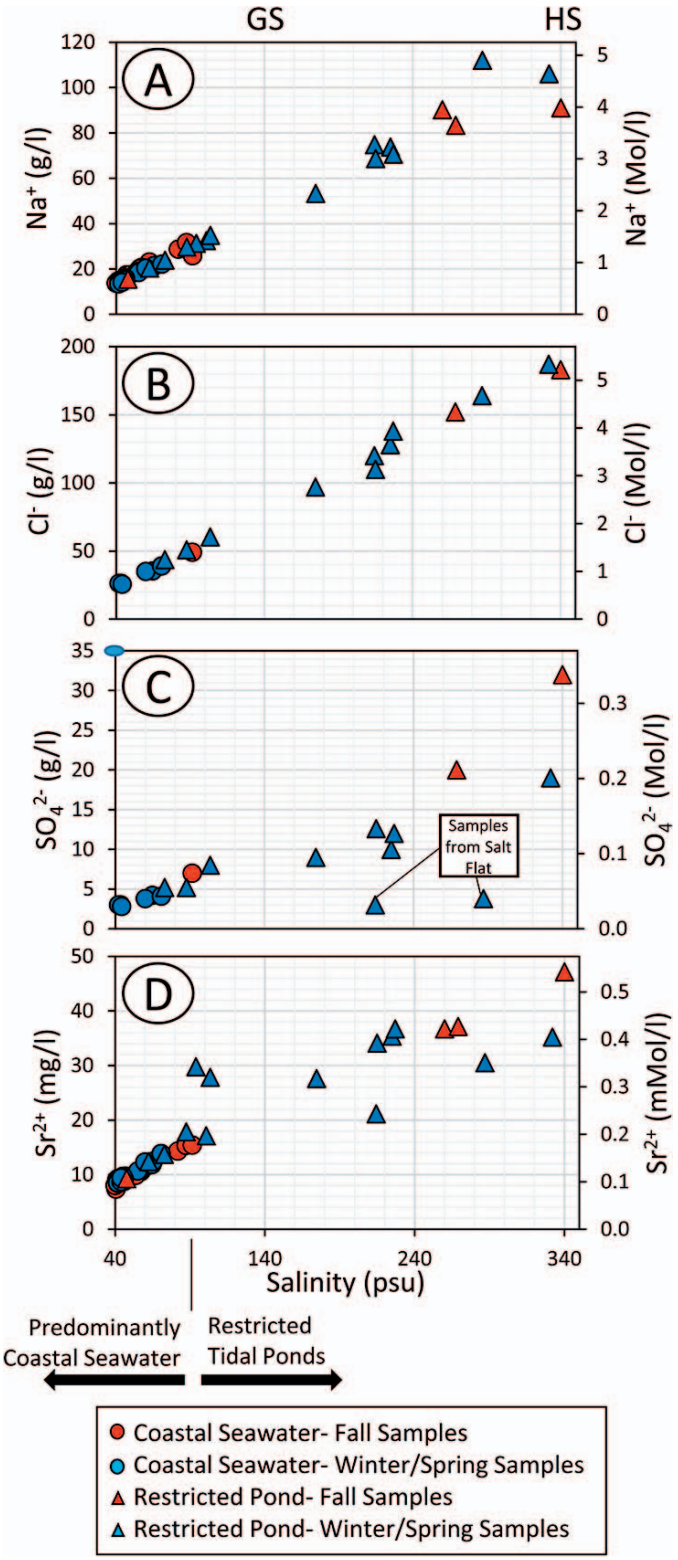

FIG. 6.—Trends in **A)** Na^+, **B)** Cl^-, **C)** SO_4^{2-}, and **D)** Sr^{2+} with varying salinity for fall and winter/spring water samples. See text regarding samples from salt flat. "GS" and "HS" show expected salinity during seawater evaporation for gypsum and halite saturation respectively (Warren 2006).

(Fig. 6C). Two samples that fall significantly below the trend are from the same tidal pond (samples ISSF-1a and ISSF-1b; Supplemental Table S1) identified above as having anomalous alkalinity. Likewise Sr^{2+} generally increases from ~ 10 to ~ 50 mg/l over the salinity range (Fig. 6D). Of note are two samples at ~ 100 psu salinity that fall above the general trend, and the two samples from ISSF-1 tidal pond, as with sulfate, that fall below the trend. K^+ concentration increase from ~ 500 mg/l to ~ 6600 mg/l as salinity rises from 40 through 340 psu. Two low outliers are noted (Fig. 7A) also from the ISSF-1 pond.

The concentrations of Mg^{2+} and Ca^{2+}, as well as their molar ratios, vary as a function of salinity (Fig. 7B, C). Mg^{2+} increases with salinity from ~ 1600 mg/l to ~ 21000 mg/l between 40 and 340 psu (Fig. 7B). The two tidal pond ISSF-1 samples fall significantly below this trend. The relationship between Ca^{2+} and salinity is more complex. Ca^{2+} increase linearly from ~ 500 mg/l to 1,100 mg/l between 40 and 90 psu. At salinities near 100 psu Ca^{2+} increases markedly to 1,900 mg/l before generally decreasing with further increase of salinity back to ~ 500 mg/l at 340 psu (Fig. 7C). The two samples that fall well above this decreasing trend are from tidal pond ISSF-1 (Supplemental Table S1). Finally, the molar Mg/Ca ratio increases from ~ 5 at 40 psu to ~ 90 to 340 psu salinity (Fig. 7D). Again, two samples that fall significantly below this trend are from tidal pond ISSF-1.

$\delta^{18}O$ and δD of Natural Surface Waters.—The $\delta^{18}O$ and δD of coastal seawater, restricted-tidal-pond water, as well as fresh-pond water are reported in Supplemental Table S1 and plotted in Figure 8A (n = 55). Samples taken during fall and winter/spring show similar values, and taken as a set the isotopic compositions range between +1 and +13 per mil for $\delta^{18}O$, and +10 and +65 per mil for δD. $\delta^{18}O$ and δD show positive correlation with a slope of 4.6 and an R^2 of 0.94 (n = 55) with no significant seasonal variation. $\delta^{18}O$ of coastal seawaters and tidal pond waters of less than ~ 100 psu correlate positively with salinity (Fig. 8B) with a slope of 0.12 and an R^2 of 0.96 (n = 48). Restricted-pond waters of greater than 100 psu salinity exhibit poor correlation between salinity and $\delta^{18}O$ values.

Carbonate and Gypsum Saturation States.—Calculated saturation indexes (SI) for dolomite, low-Mg calcite, aragonite, and gypsum are shown in Figure 9. Calcite and aragonite SI for open Arabian Gulf waters are ~ 1, rising with increased concentration to ~ 1.5 by near 300 psu, before falling to approximately 0.8 for the two higher-salinity samples near halite saturation. Likewise, dolomite SI for open gulf waters is ~ 3 but rises to ~ 4.3 during concentration, remaining elevated through 340 psu. Normal gulf water is undersaturated with respect to gypsum (SI < 0). As waters are concentrated the degree of gypsum undersaturation decreases until > 100 psu; at which point the waters become supersaturated with respect to gypsum.

Elemental and Stable-Isotope Composition of Cerithid Gastropods and Aragonitic Mud

$\delta^{18}O$ and $\delta^{13}C$ of Pirenella Gastropods and Aragonitic Mud.—For the fall and winter/spring sampling seasons $\delta^{18}O$ values of whole *Pirenella cingulata* gastropods fall between –2 and +6‰, and $\delta^{13}C$ values vary between –1 and +5‰ (Table 1, Fig. 10A). In general, $\delta^{18}O$ and $\delta^{13}C$ values positively correlate ($R^2 = 0.43$; n = 32). Samples of aragonitic mud (n = 11) from the Inland Sea system fall on the same trend (Table 2). The $\delta^{18}O$ of gastropod shells strongly correlates (slope near 1) with that of the waters from where they were collected for both fall and winter/spring sample sets ($R^2 = 0.97$ (n = 15) and $R^2 = 0.85$ (n = 12) respectively) (Fig. 10B). Compared to fall samples, however, winter/spring gastropods have ~ 1‰ higher shell $\delta^{18}O$ values for a given seawater $\delta^{18}O$. Figure 10C shows that there are also positive seasonal correlations between shell $\delta^{18}O$ and

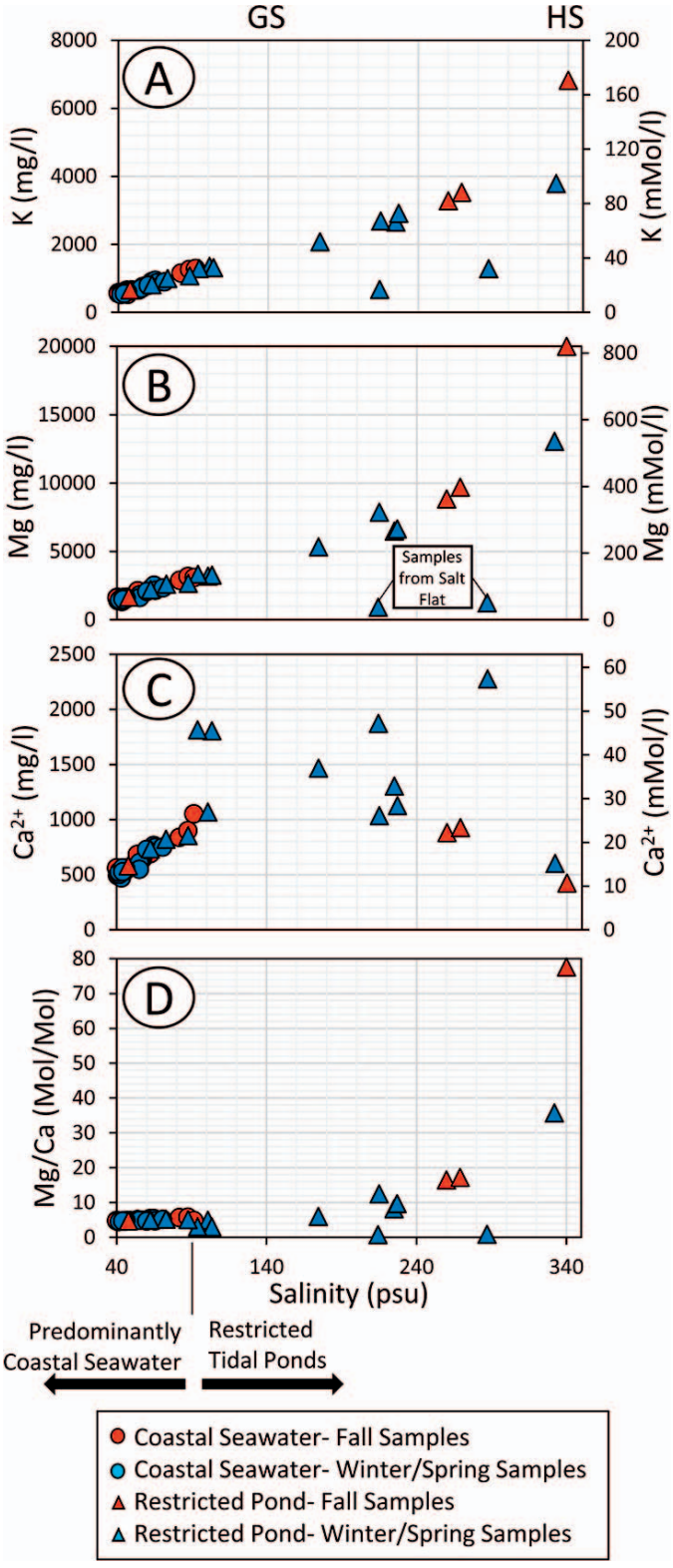

FIG. 7.—Trends in **A)** K^+, **B)** Mg^{2+}, **C)** Ca^{2+}, and **D)** molar Mg/Ca ratio with varying salinity for fall and winter/spring water samples. "GS" and "HS" show expected salinity during seawater evaporation for gypsum and halite saturation respectively (Warren 2006). See text regarding samples from salt flat.

seawater salinity, with slopes of 0.10 ($R^2 = 0.90$, n = 15) for fall and 0.13 ($R^2 = 0.86$, n = 12) for winter/spring.

Ca^{2+} and Sr^{2+} Concentrations of Pirenella Gastropods.—The Ca^{2+} and Sr^{2+} concentrations of *Pirenella cingulata* gastropods are reported in Table 1. Ca^{2+} accounts for ~ 40 weight % of the aragonite shell. Sr^{2+} content varies between 800 and 1400 ppm. Sr^{2+} normalized to Ca^{2+} concentrations are also reported in Table 1.

INTERPRETATION

Evolution of Marine Waters During Evaporation: Mineral Precipitation and Dissolution Reactions

The pH of waters below 60 psu is highly variable, which is not uncommon for unrestricted marine systems (Hofmann et al. 2011). With increasing evaporation the alkalinity and pH of Qatar coastal and restricted-tidal-pond waters change antithetically (Fig. 5A, C). As pH increases, alkalinity decreases to salinities of ~ 90 psu. Above this salinity pH decreases as alkalinity increases. Outliers include one sample at 62 psu with anomalously high pH and DO, and two samples (214 and 287 psu) from the same pond with their alkalinity readings falling well below the trend. With respect to the general trends, the most likely explanation for the initial decrease in alkalinity is the precipitation of aragonite driven by increasing SI (Fig. 9). In the Inland Sea channel and lagoon system (Fig. 2), where coastal waters are concentrated beyond 60 psu (Fig. 4), coated grains are forming along the western shoreline of the outer lagoon (Fig. 11A), and aragonite cement forms clasts commonly found in the subtidal muddy sediments of the Inland Sea (Fig. 11B). Aragonite crystallization is likely driven by increasing ionic strength, causing CO_2 levels to fall (Markham and Kobe 1941), and therefore pH to rise during evaporation. Lazar and Erez (1992) observed a 50% decrease in CO_2 in evaporation-pan waters of a solar salt production plant during initial brine concentration up to ~ 140 psu.

In tidal ponds, as salinities increase beyond 90 psu, the alkalinity rises in large part as a result of evaporative concentration. However, the observed pH drop from ~ 8.6 (at ~ 90 psu) to ~ 7.6 (at 340 psu) may also result in carbonate dissolution. Whereas the effect of mixing meteoric water and seawater in winter/spring samples is uncertain, the phenomenon of decreasing pH is observed in evaporating waters apparently not affected by meteoric influence (fall samples). The increased H^+ activity during early stages of seawater evaporation has been reported from laboratory seawater experiments by Lazar et al. (1983), who interpret this to result from changes in the dissociation constants for carbonate acid as ionic strength increases. They demonstrated that continued evaporation of seawater caused a lowering of pH and related undersaturation with respect to aragonite. An interpretation of aragonite dissolution is supported by a marked increase in [Ca^{2+}] (Fig. 7C) and [Sr^{2+}] (Fig. 6D) immediately following evaporative concentration above ~ 90 psu. The aragonite undersaturation is not apparent in the saturation calculations, perhaps because aragonite dissolution buffers the pH change more or less instantaneously (i.e., between sample periods). Notably, the Mg^{2+} concentrations are unchanging in waters with the elevated Ca^{2+} and Sr^{2+}. This suggests that dolomitization is not occurring. As evaporation continues to > 100 psu, [Ca^{2+}] decreases as a result of observed gypsum precipitation (Fig. 7C), a decrease also noted by McCaffrey et al. (1987) of brines from solar salt production sites at similar evaporative concentrations. Sulfate concentration continues to increase in spite of gypsum precipitation (Fig. 6C) as a result of the chemical divide caused by its higher initial concentration relative to [Ca^{2+}] (Hardie and Eugster 1970). Above 300 psu, Na^+ begins to decline as a result of halite precipitation (Fig. 6A) as also observed.

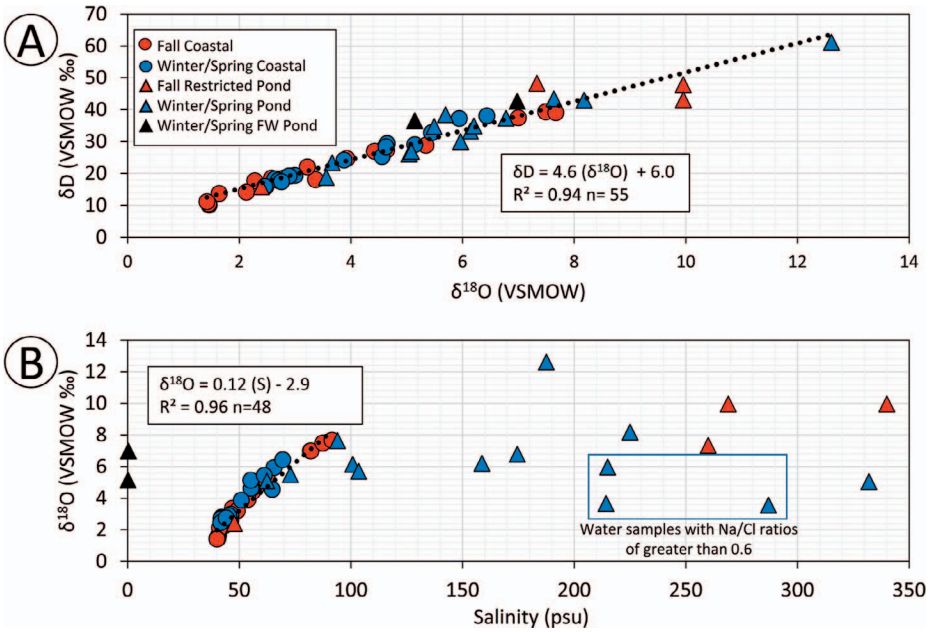

FIG. 8.—**A)** Relationship between $\delta^{18}O$ and δD for water samples in this study. **B)** Variation in $\delta^{18}O$ with salinity for natural waters samples in this study. The freshwater-pond samples we collected after several weeks of evaporation following a significant rainfall event. S, salinity.

Outliers to the general trends described above are observed. Firstly, whereas almost all tidal ponds sampled for this study lacked vegetation (although some had microbial mats), an outlier with anomalously high pH (8.6) for its measured salinity (62 psu) (Fig. 5, white triangle) was sampled in a mangrove forest, and its elevated pH and DO is likely owed to ongoing photosynthesis. Secondly, two samples taken at different times from the same tidal pond (ISSF-1a and ISSF-1b) also fall off many of the general trends described above (Figs. 5–7; salinity 214 and 287 psu). The pond formed on a salt flat that was likely stranded as sea level fell from ~ +3 m 6000 years ago to its current position (Engel and Brückner 2014). The salt flat is rarely flooded by marine waters (it had remained dry during the summer of 2016), but was flooded by rain water during a storm in November of 2016. Sampling was undertaken in mid-December (ISSF-1a) and again late December (ISSF-1b) (Supplemental Table S1). These waters were notably different than other pond waters in that they smelled of sulfide, an observation supported by low sulfate concentration (Fig. 6C; waters of $>$ 200 psu with sulfate of $<$ 5000 mg/l). In spite of this, measured oxygen levels were not anomalously low (Fig. 5B), perhaps indicating that measured waters were a mixture of tidal-pond water and pore waters disturbed during sampling by wading. Other unique chemical attributes of these samples relative to the general trends in the other tidal-pond waters include: lower Sr^{2+} (Fig. 6D), lower K^{+} (Fig. 7A), low Mg^{2+}, (Fig. 7B), and elevated Ca^{2+} (Fig. 7C). The high salinities of these samples are the result of meteoric dissolution of salts in the dry flat, as evidenced by the Na/Cl weight ratio (Supplemental Table S1) of ~ 0.65 (or a 1:1 molar Na:Cl ratio), whereas the normal seawater Na/Cl weight ratio is 0.55

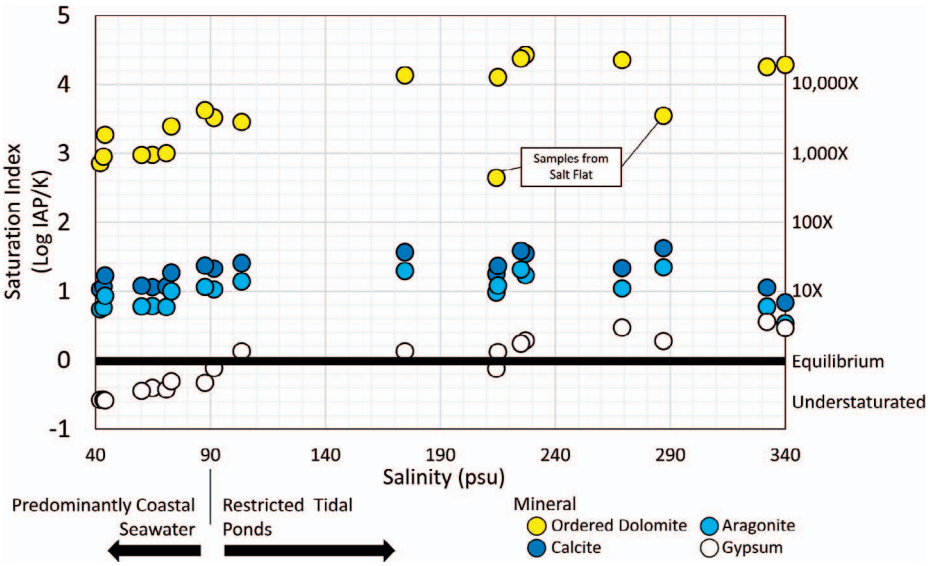

FIG. 9.—Saturation indexes for dolomite, calcite, aragonite, and gypsum for coastal water and tidal ponds as a function of salinity.

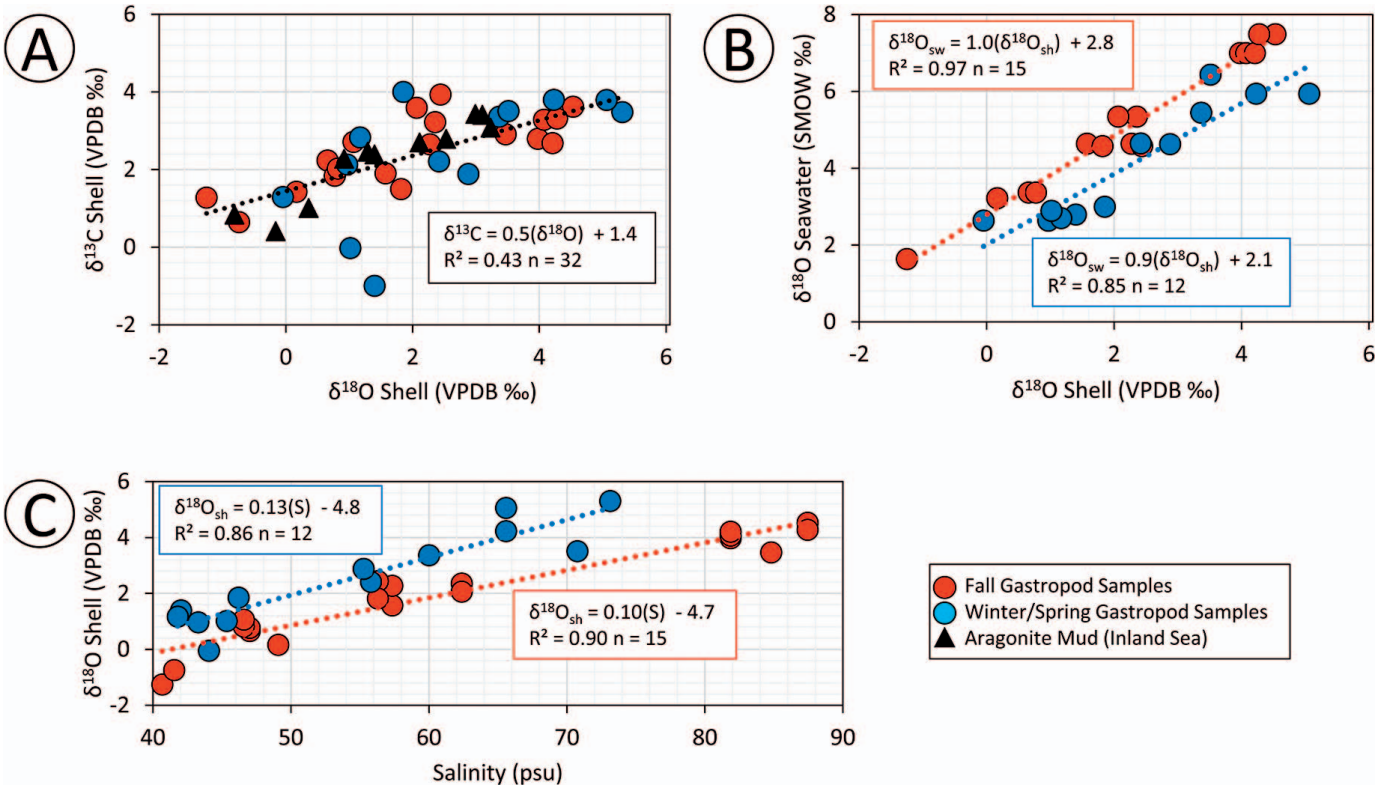

FIG. 10.—Trends for **A)** $\delta^{18}O$ vs. $\delta^{13}C$ from shells of living gastropods and aragonitic mud collected during water sampling, **B)** $\delta^{18}O$ gastropod shell vs. $\delta^{18}O$ of seawater at the time of collection, and **C)** $\delta^{18}O$ gastropod shell vs. measured ambient seawater salinity.

(McCaffery et al. 1987). Low sulfate concentration is likely caused by the anaerobic bacterial breakdown of buried microbial mats, which are observed in the pond under ~ 30 cm of dune-sourced clastic sand mixed with carbonate mud. The low [Mg^{2+}] might, in part, be explained by a lack of Mg salts in the pond before meteoric flooding. This is supported by relatively low potassium levels in the pond, as potassic salts typically form during or after seawater concentration to Mg-salt precipitation (Warren 2016). However, the Mg:Ca ratio is less than unity, falling below the trends of both brines formed from evaporation of seawater (fall samples), and other brines likely influenced by meteoric dilution and subsequent salt dissolution (winter/spring samples). For instance, sample ISTP-2e has Na:Cl ratios indicative of halite dissolution by meteoric waters, but Mg:Ca ratio of 12.5 (Supplemental Table S1). The low Mg levels in the sulfate-reducing pond can therefore be explained by formation of very high-Mg calcite or of dolomite. The elevated Ca^{2+} levels (including the highest measured in the study) relative to the trend of evaporating marine (fall) and mixed (winter/spring) waters would seem to indicate that such dolomite forms by replacement of calcite, although, in these reducing waters, gypsum dissolution could also explain the observation. XRD of sediments bedded within the degrading mat indicates the presence of small amounts of very high-Mg calcite or perhaps poorly ordered dolomite to be present within the muddy sand. The small amounts of the Ca-Mg-carbonate phases in these samples makes it difficult to identify an accurate index of the ordering peaks, which are necessary evidence of dolomite (Kaczmarek et al. 2017). If the phase identified is VHMC, it could represent an initial phase of crystallization from which well-ordered dolomite forms, as seen in high-temperature experiments (e.g., Kaczmarek and Thornton 2017). The possibility of replacive dolomite is currently under investigation. The relatively low Sr^{2+} levels are ambiguous because the distribution coefficient of Sr^{2+}into dolomite is less than unity (Vahrenkamp and Swart 1990).

TABLE 2.—*Stable isotopic composition of aragonite mud taken from sampling transects of the Inland Sea channel and lagoon system.*

Map Location	$\delta^{13}C$ (‰ VPDB)	$\delta^{18}O$ (‰ VPDB)
1	2.7	2.1
2	3.4	3.0
3	2.3	0.9
4	2.5	1.3
5	3.4	3.1
6	3.1	3.2
7	0.4	–0.16
8	1.0	0.4
OL1	2.8	2.5
OL2	2.4	1.4
OL3	0.8	–0.81

Evolution of Marine Waters during Evaporation: $\delta^{18}O$ and δD Trends

The D-O isotopic trend revealed in this study for evaporating seawater was unexpected (Fig. 12). Expected changes to the $\delta^{18}O$ and δD of residual seawater during evaporation as reviewed by Knauth and Beeunas (1986), and based on experimental data and extrapolation from studies by Craig (1961), Craig and Gordon (1965), and Holser (1979) are plotted on Figure 12. Salinity in psu is displayed on both the Knauth and Beeunas (1986) and Qatar water trends.

During initial evaporation and concentration of sea water, ^{16}O fractionates preferentially into the vapor phase both as a function of

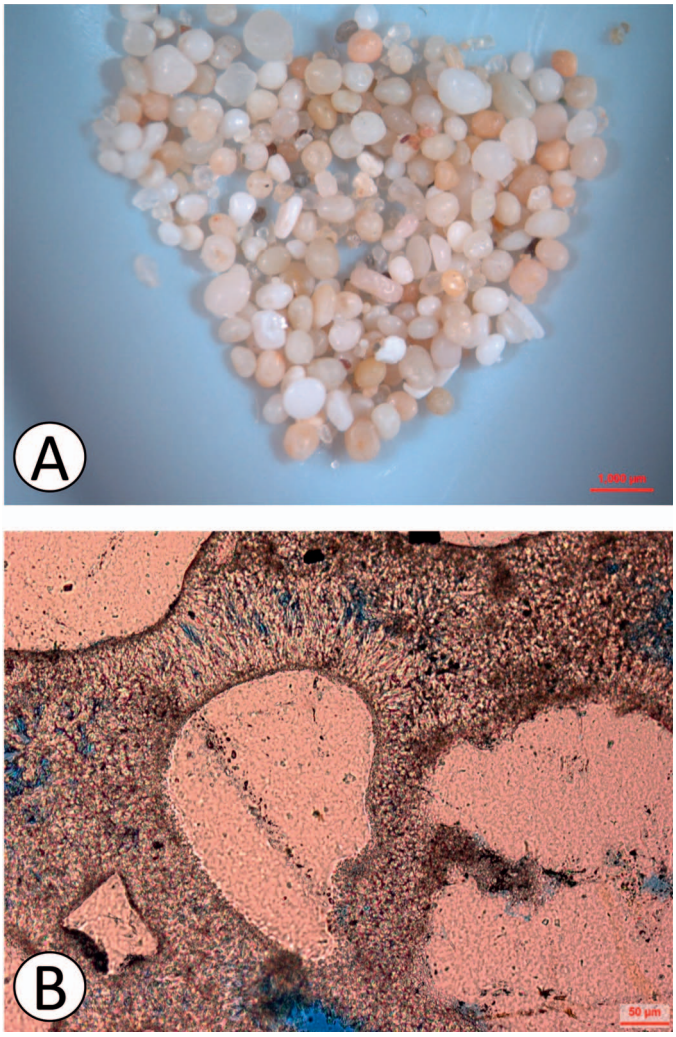

FIG. 11.—**A)** Image of coated grains collected from the western shoreline of the Inland Sea outer lagoon (see Fig. 2). **B)** Thin-section image of intraclasts from the inner lagoon of Inland Sea showing cementation of quartz sand by fibrous aragonitic cement (confirmed by XRD).

equilibrium (Rayleigh distillation) and due to differences in diffusion coefficients (e.g., Lloyd 1966), enriching residual waters in ^{18}O and D (Fig. 12). Isotopic concentration gradients across the diffusion layer between water and air also play a role, such that in more humid conditions the ^{18}O concentration gradient between the water and vapor is higher, causing increased diffusion of ^{18}O to the vapor phase, and countering equilibrium fractionation (Lloyd 1966). The role of a higher ^{18}O concentration gradient is accentuated as the seawater becomes increasingly enriched in ^{18}O during evaporation. Additionally, as evaporation continues, the vapor pressure of the water drops, and this can lead to condensation of atmospheric vapor back into the brine, causing a net decrease of $\delta^{18}O$ as water salinity increases (e.g., Lloyd (1966): Inagua example, Fig. 5). This, in part, explains the reversal in the Knauth and Beeunas (1986) isotopic trend shown in Figure 12, as concentration increases beyond 140 psu, or gypsum saturation. The roles of exchange between "hydration sphere" water and unbound water during evaporation (Holser 1979), as well as the sequestering of ^{18}O into gypsum (Gonfiantini and Fontes 1963) have both been postulated as additional explanations for the trend reversal.

For this study, it is assumed that salinities attained during the fall, at the end of dry season, directly reflect the degree of evaporation, as freshwater input is negligible. This is supported by the observation that the highest $\delta^{18}O$ values measured in fall samples are from the most saline waters (Fig. 10). Further support is lent by the Na/Cl ratios (by weight) of fall restricted-tidal-pond samples ISTP-2a (salinity = 269 psu) and ISTP-2b (salinity = 340 psu; halite observed in pond). ISTP-2a has a ratio near that expected for seawater below halite saturation ($\sim$ 0.55) (McCaffery et al. 1987), in line with its measured salinity. ISTP-2b has a ratio lower than 0.55, as expected for marine waters precipitating halite (McCaffery et al. 1987), since Na and Cl are removed from the fluid on a one-to-one mole basis. Winter/spring tidal-pond samples were collected after significant rainfall, and are likely a mixture of marine-derived water and rainwater. These mixed waters tend to fall below the fall $\delta^{18}O$-salinity curve for pure-marine evaporated waters due to dilution (Lloyd (1966); Fig. 6, therein). Rainwaters may also dissolve residual salts precipitated in the restricted-tidal-pond basins during dry-season sea-water evaporation. Because Na and Cl are added by halite dissolution on a one-to-one mole basis (or 0.65 weight ratio), solution Na/Cl ratios increase above 0.55, as observed in three of the more saline winter/spring tidal-pond samples (Supplemental Table S1). Because these waters are saline as a result of salt dissolution, but not greatly evaporated, they fall below the trend of increasing $\delta^{18}O$ with salinity (Fig. 8).

For Qatar waters, both $\delta^{18}O$ vs δD values apparently continue to rise beyond the degree of evaporation required for halite saturation of strictly marine waters (Figs. 8A, 12). This assumption is based on sample ISTP-3b (a highly evaporated springtime mixed marine–meteoric water; the last vestige of an evaporating tidal pond), which has higher $\delta^{18}O$ and δD values than the fall halite-saturated strictly marine pond (ISTP-2b). To our knowledge the highest $\delta^{18}O$ and δD values (greater than +12‰ and +60‰ respectively) reported in this study fall above the envelope of those reported for global meteoric waters (Craig 1961) and marine-derived brines (Major et al. 1992), and reaching $\delta^{18}O$ values 7‰ higher than brines of similar salinity taken from Qatar sabkha pits (Lloyd 1966). Brines with $\delta^{18}O$ values approaching 12‰ have been found in open solar ponds evaporating in low-humidity environments, such as Solar Lake, adjacent to the Red Sea, where humidity is on average 30% (Aharon et al. 1977).

One explanation for the differences in isotopic evolution in pond waters reported in this study compared to those of local sabkha pits examined by Lloyd (1966), who showed lower $\delta^{18}O$ as waters concentrated above $\sim$ 150 psu, might be the nature of the evaporation system. Evaporation in ponds occurs in open air, where the atmosphere is consistently moved by the winds, and represents an infinite reservoir. The air does not greatly evolve as a consequence of the pond evaporation. This means that there is minimal molecular exchange, and water vapors enriched in ^{16}O diffuse quickly. Similarly, open-air evaporation experiments reported by Lloyd (1966) created evaporated waters of $\sim$ 9‰ or higher. Compared to open pond evaporation, sabkha pit waters are in large part evaporated within sediments (a result of evaporative pumping (Hsu and Siegenthaler 1969)). Presumably in this setting the vadose air is stagnant, more humid (as air is not flushed quickly during evaporation), and able to condense vapor back into the brine. Thus, an intrasediment system would more likely limit the amount of isotopic fractionation achievable. That stated, data on open salt-pans from Lloyd (1966) (Inagua and San Francisco Bay) show depleted $\delta^{18}O$ values similar to the sabkha-pit samples, so other factors must be important. Notably, there does not seem to be an impact on the slope of $\delta^{18}O$–δD trend for Qatar sea and pond waters either associated with differences in humidity between northern vs. southern Qatar, or differences in humidity between seasons (Figs. 3C, 8).

Comparative Chemistry of Seawater and Gastropod Shells

Pirenella cingulata is abundant along the open sand and mud flats of the Qatar coasts. These gastropods can tolerate a wide range of water salinity

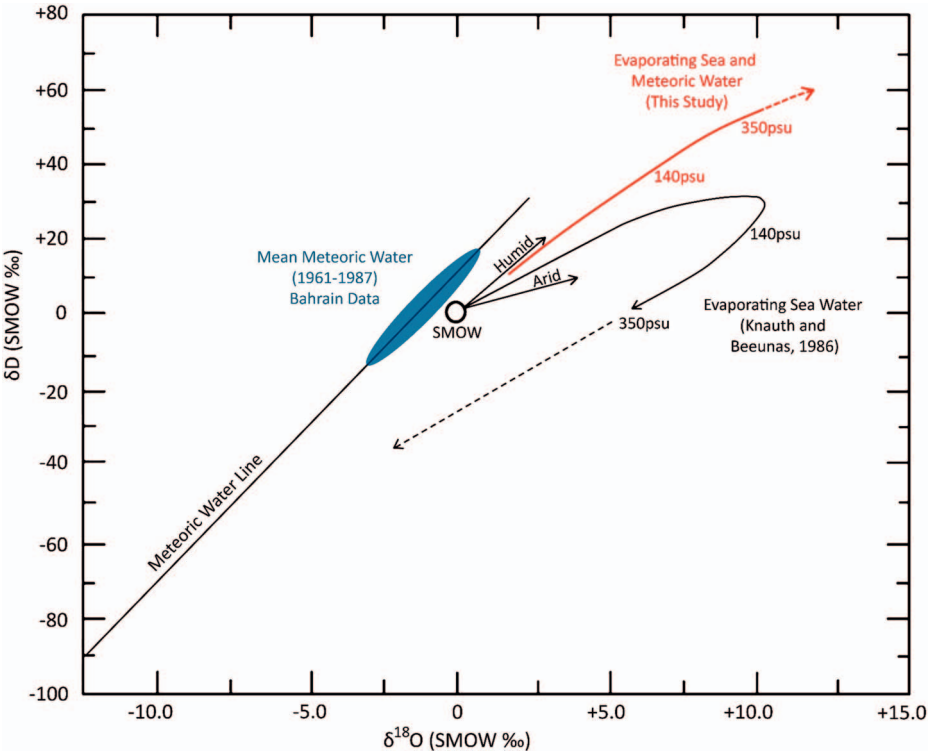

FIG. 12.—Trends of $\delta^{18}O$ vs. δD for waters of this study and those published by Knauth and Beeunas (1986). Seawater salinity is shown for both trends. For this study, salinity data are from fall sampling (end of dry season) of evaporating marine waters with no apparent influence by rain water. Assumed isotopic composition of local rain waters is also shown based on Bahrain data collected between 1961 and 1987 (IAEA 1992). Yearly mean values (per mil) over that period were –0.97 ± 1.99 for $\delta^{18}O$ and +4.6 ± 11.8 for δD.

and temperature (Annandale and Kemp 1916; Jutting and Van 1956; Reid and Ozawa 2016). They feed on fine organic matter that settles on the sediments (Sreenivasan and Natatajan 1991), and in Qatar are commonly observed grazing at the edges of algal mats. Based on studies mainly in India, these animals can reproduce year around, but growth is faster in the summer and slower in the winter (Rao and Rao 1983), with optimal growth temperature range of 28–34°C (Sreenivasan 1985). The life expectancy of this species is ~ 1 year (Reid and Ozawa 2016).

The $\delta^{18}O$ of whole *Pirenella cingulata* gastropods correlates well with that of the seawater from which each was sampled (Fig. 10B). The ~ 1‰ offset in trends observed when comparing samples collected during the fall with those collected during the winter/spring is likely a reflection of differences in seawater temperature during shell growth not long before collection. Samples collected during the fall grew to a large degree during hot summer months (May–September) when water temperatures averaged ~ 32°C (Fig. 3). Samples collected during winter/spring had significant growth during October–April, when water temperatures there probably averaged ~ 22°C based on regional air temperature (Fig 4). The average water temperature during growth of an aragonitic shell (assuming near-equilibrium) can be calculated using Dettman et al. (1999) after Grossman and Ku (1986):

$$\mathrm{SST}(^{\circ}\mathrm{C}) = 20.6 - 4.34(\delta^{18}O_S - (\delta^{18}O_W - 0.27)) \quad (1)$$

where $\delta^{18}O_S$ is for shell material in VPDB, and $\delta^{18}O_W$ is for seawater in SMOW. Using an average $\delta^{18}O_S - \delta^{18}O_W$ offset of ~ 3‰, the calculation yields an average fall growth temperatures of ~ 32°C. The winter/spring samples, assuming an average $\delta^{18}O_S - \delta^{18}O_W$ offset of ~ 2‰, yields an average of ~ 28°C. The fall-sample calculation is consistent with measured summer sea-surface temperatures, whereas the winter/spring calculation is ~ 6°C higher than expected given average sea-surface temperatures across that time interval. This may reflect a bias for shell growth during warmer months (Sreenivasan 1985).

Similarly, the relationship between seawater salinity and the $\delta^{18}O$ of the gastropods shows an offset by season interpreted to reflect the influence of growth temperature on $\delta^{18}O$ fractionation (Fig. 10C). This effect aside, there is a strong correlation ($R^2 \geq 0.85$) between water salinity and shell $\delta^{18}O$, reflecting their mutual control by degree of evaporation in the shallow subtidal waters. Isotopic and salinity enrichment ratios are between 0.10 (summer) and 0.13 (winter/spring). These values are consistent with those reported by Craig and Gordon (1965) of 0.11 for low-latitude shallow ocean waters, as well as Dufour et al. (1998) of 0.14 for fish otoliths, in spite of the much more limited levels of evaporation (marine salinities < 45 psu) in these studies.

There is no obvious relationship of decreasing shell $\delta^{18}O$ with increasing pH in this study, which has been observed in foraminifera culture experiments (Spero et al. 1997; Zeebe 1999). However, most shells were collected in waters between 8.0 and 8.5 pH, which would correspond with only an approximately 0.5‰ expected $\delta^{18}O$ variation as a result of differences in isotopic fractionation in dissolved carbonate species. Such variation is much less than the ~ 5.0‰ variation expected (and observed) for changes in seawater $\delta^{18}O$ as a result of evaporation given the measured salinities observed during shell collection.

Positive correlation between the $\delta^{18}O$ and the $\delta^{13}C$ of shell material (Fig. 10A) has been observed previously in evaporative marine systems (e.g., Rivers et al. 2009). In shallow, evaporative, restricted systems, where replenishment of open-marine carbon is inefficient, photosynthesis can sequester ^{12}C into organic matter as shown during early stages of evaporation experiments by Lazar and Erez (1992). Rather than returning to the carbon pool during decay, such organic carbon may be exported from the system by seasonal saline currents as particulate matter (e.g., Smith and Veeh 1989).

Lastly, Sr^{2+} concentrations in gastropods exhibit no correlation with either ambient oceanographic measurements at the time of gastropod collection, or with stable-isotope measurements of the gastropod shell (Fig. 13). Further, there is no significant difference in the Sr^{2+} concentration in shells taken during the two collection seasons, as would be expected given the seasonal temperature differences both observed and interpreted based on isotope data. Typically Sr^{2+} content in biogenetic aragonite correlates

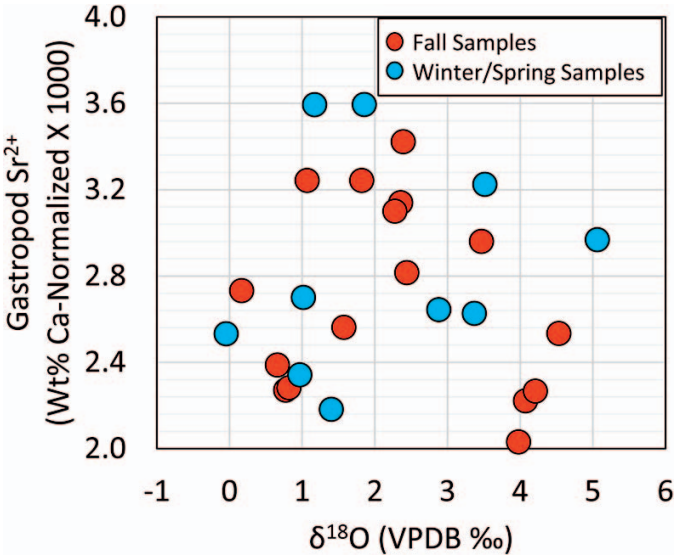

FIG. 13.—Ca-normalized strontium content vs. $\delta^{18}O$ of shells from gastropods collected (live) during water sampling.

antithetically with water temperature during growth (e.g., Smith et al. 1979). Why this does not appear to be the case regarding *Pirenella cingulata* is uncertain, but may reflect a biologic control.

IMPLICATIONS

The concentration of marine waters by evaporation, dissolution of marine-derived salts by meteoric waters, and influence of microbial breakdown of organic matter lend themselves to reactions that can cause carbonate precipitation, dissolution, or replacement. It has long been recognized that initial evaporation of seawater drives early marine cementation (e.g., Evamy 1973), although early marine cementation is widespread in the Arabian Gulf, including in waters with only a marginal degree of concentration (Shinn 1969). In spite of apparent ongoing precipitation, sediments of the Inland Sea channel and lagoon system, where subtidal waters concentrate to ~ 90 psu, are far from well lithified. In the grainy channel and delta areas (Fig. 2), the sediments are mostly quartz sand. Although coated grains and intraclasts are present, they make up less than approximately 10% of the observed assemblage, and no hardgrounds have been identified. The carbonate muds of the inland sea are still mostly soft, although thin (< 1 cm), patchy hardgrounds are observed. Significant lithification in the marine realm, which is observed along the windward northern coast of Qatar in the form of beachrocks, would seem more a function of wave-generated water agitation (Gischler and Lomando 1997) than the concentrated availability of chemical constituents.

Early replacive dolomitization associated with evaporite formation is common in the rock record of Qatar (e.g., the Eocene Rus Formation; Al-Saad 2003). Such dolomitization is consistent with the salinity reflux model of Adams and Rhodes (1960). This might be expected given the saturation state of dolomite increases ~ 20× (Fig. 9), in part reflecting the increasing Mg/Ca ratio (Fig. 7D). Some dissolution of aragonite is suggested by an increase in Ca^{2+} (Fig. 6D) and Sr^{2+} (Fig. 7C) at ~ 90 psu, and is associated with an initial pH drop during seawater concentration (Fig. 6A). This pH change and associated aragonite dissolution was observed in laboratory seawater evaporation experiments by Lazar et al. (1983). Such Mg^{2+}-rich, aragonite-corrosive waters were postulated by Sun (1992) and Rivers et al. (2012) to be responsible for the replacive dolomitization commonly found in association with ancient evaporative marine systems. The dissolution observed in the tidal ponds of Qatar, however, appears minor, as the alkalinity remains low (Fig. 5C). Importantly, there is no evidence of lower Mg^{2+} levels associated with the pH fall at 90 psu that would reflect ongoing replacive dolomitization (Fig. 7B).

The only waters sampled in this study that show potential evidence of ongoing replacive dolomitization were meteoric in origin (samples ISSF-1a and 1b; Supplemental Table S1). These waters were taken from a flooded salt flat in the weeks following significant rainfall. One obvious difference between this pond and others sampled for this study was its reducing nature (low sulfate levels; Supplemental Table S1), likely associated with degrading microbial mats discovered several decimeters below the gypsum-rich dune sand and carbonate mud that floors the pond. The potential importance of microbial substances in overcoming inhibition of dolomite nucleation has been documented (e.g., Bontognali et al. 2010; Petrash et al. 2017). Studying a Qatar sabkha, Brauchli et al. (2015) found there was dolomite enrichment in sediments associated with the presence of organic matter resulting from microbial-mat formation. It is notable, however, that both the Inland Sea and other tidal ponds sampled in this study are the sites of ongoing and prolific microbial mat growth. Therefore it appears that the mere presence of microbial mats is not enough to cause dolomitization to a degree that results in significant changes to the Mg/Ca ratio of the overlying water. Anoxic breakdown of the organic matter may be a crucial factor in replacive dolomitization, for two reasons. First, the presence of H_2S has been shown to catalyze dolomite formation (Shen et al. 2014). Second, the subsequent oxidation of H_2S results in acidification of pore waters and the lowering of calcium-carbonate saturation levels (Morse and MacKenzie 1990). Whereas these low calcium-carbonate saturation levels are not evident from calculations of pond-water saturation (Fig. 9), markedly elevated Ca^{2+} concentrations are (including the highest measured in the study), and are suggestive of aragonite dissolution. It is likely that the low calcium carbonate saturation occurs in pore waters proximal to microbial material. Such low saturation levels may be necessary to drive dissolution–precipitation reactions causing replacive dolomitization.

The strong correlation between the $\delta^{18}O$ of seawater and of *Pirenella* gastropods (Fig. 10B) suggests that these shells are potentially useful chemical archives for the isotopic chemistry of ancient oceans. The positive correlation between the $\delta^{18}O$ and $\delta^{13}C$ values of *Pirenella* shells (Fig. 10A) has also been observed in shells from evaporative passive margin-settings. Rivers et al. (2009) showed that the $\delta^{18}O$ and $\delta^{13}C$ values of large benthic foraminifera tests (*Marginopora vertibralis*) from the southern Australian margin exhibited positive correlation. They interpreted these protists to have formed in shallow evaporating seawater during marine isotope stages (MIS) 2 and 3. Previously unpublished data from that study show Cerithioidea *Batillaria* gastropod shells have a similar positive correlation (Table 3, Fig. 14). These intertidal and near-shore forms (Ozawa et al. 2009) were recovered from deep (> 30 m) open shelves. As with the large benthic foraminifers, they likely formed in a shallow evaporating ocean that covered the shelves during MIS 2 and MIS 3, archiving the ^{18}O and ^{13}C composition of those waters. Using the winter/spring $\delta^{18}O$-salinity relationship for *Pirenella cingulata* shells from the Qatar study (since southern Australia is a cooler-water realm), the $\delta^{18}O$ variation in the Cerithioidea *Batillaria* shells (0.6–3.4 per mil) indicates salinities varied between 40 and 60 psu during their formation, in fairly good agreement with interpreted salinity range based on the large benthic foraminifera study (38–56 psu; Rivers et al. 2009).

Importantly, the variability in $\delta^{18}O$ and $\delta^{13}C$ of aragonite shells and muds as related to evaporation in these shallow arid environments is significant (6‰ and 3‰, respectively; Figs. 10A, 14), encompassing much of the secular variation through the Phanerozoic (Veizer et al. 1980; Veiser et al. 2000). Therefore, in such settings, local variations in marine restriction, largely controlled by paleotopography, will likely result in

TABLE 3.—*Location and isotopic composition of Cerithioidea gastropod samples* (Batillaria) *from the southern Australian margin.*

Sample Name	Lattitude (S)	Longitude (N)	Depth (m)	$\delta^{13}C$ (‰ VPDB)	$\delta^{18}O$ (‰ VPDB)
GAB_102	34°2′49″	122°1′53″	35.5	2.6	3.6
GAB_070	34°5′8″	124°23′4″	73	1.1	2.0
GAB_052	34°23′60″	125°11′0″	71	1.0	1.8
GAB_055	34°43′14″	125°18′10″	61	0.6	0.7
GAB_058	34°51′47″	125°57′44″	65	0.9	1.1
GAB_032	33°19′57″	128°28′54″	54	1.3	1.3
GAB_007	32°9′31″	129°0′19″	42	1.3	1.4
ACM_087	34°51′58″	130°52′11″	106	1.5	1.3
ACM_067	34°35′55″	132°51′7″	94	3.4	3.0
ACM_029	37°55′60″	137°3′8″	57	0.7	1.7
VH89_034	37°18′16″	138°22′27″	61	1.2	1.7
ACM_057	34°15′55″	133°15′58″	94	1.7	2.6
VH89_046	37°5′30″	138°36′56″	67	1.6	2.0
VH89_040	37°50′4″	139°25′52″	41	1.6	2.6
ACM_056	35°46′26″	132°58′48″	121	1.8	2.8
ACM_039	36°50′53″	134°46′12″	124	1.9	3.7
ACM_034	37°52′30″	135°53′49″	177	2.0	3.7
ACM_008	39°43′52″	140°44′37″	131	2.2	3.4
ACM_008	39°43′52″	140°44′37″	131	2.3	3.3

isotopic variability to a degree that overwhelms regional- or global-scale excursions, potentially rendering carbon and oxygen "isotope stratigraphy" ineffective.

Finally, based on this study and assuming equilibrium, dolomite forming in the presence of waters concentrated to the point of gypsum or halite saturation in open-air settings would be expected to have $\delta^{18}O$ values on the order of ~ 5–10 per mil higher than that forming from unevaporated seawater. Modern and ancient (Cenozoic and Mesozoic) dolomites interpreted to have formed in evaporative settings generally display $\delta^{18}O$ of less than 5‰, with the notable exception of Coorong-type dolomites that have $\delta^{18}O$ values between +4 and +8 (Warren 2000). Since the oxygen isotopic composition of seawater during the Mesozoic and Cenozoic is broadly similar to that of the modern ocean (Veizer et al. 1997), either Qatar open pond waters are not representative of those typically associated with evaporative dolomitization (although sabkha pore waters might be), or the initial $\delta^{18}O$ of evaporative dolomites is reset in the presence of less-evaporated waters after formation.

CONCLUSIONS

A multi-season Qatar-wide study of coastal sea and pond waters shows that concentration by evaporation drives minor cementation, followed by minor aragonite dissolution, before gypsum and halite precipitation. Evidence of significant dolomitization based on expected Mg^{2+}/Ca^{2+} ratios was mostly absent, but the precipitation of very-high-Mg calcite or poorly ordered dolomite is potentially occurring in the presence of anaerobic bacterial breakdown of buried microbial mats. Based on water chemistry, this reaction appears calcium-carbonate-replacive, and is interpreted to be driven by H_2S generation and oxidation.

During evaporation, Qatar coastal waters exhibit higher $\delta^{18}O$ vs. δD values than measured previously in similar studies. The high values are interpreted to reflect pond evaporation in the open atmosphere, as opposed to within ground air (pore systems in the unsaturated zone) during evaporative pumping within the sabkha. The slope of the $\delta^{18}O$ vs. δD trend does not show dependence on seasonal humidity.

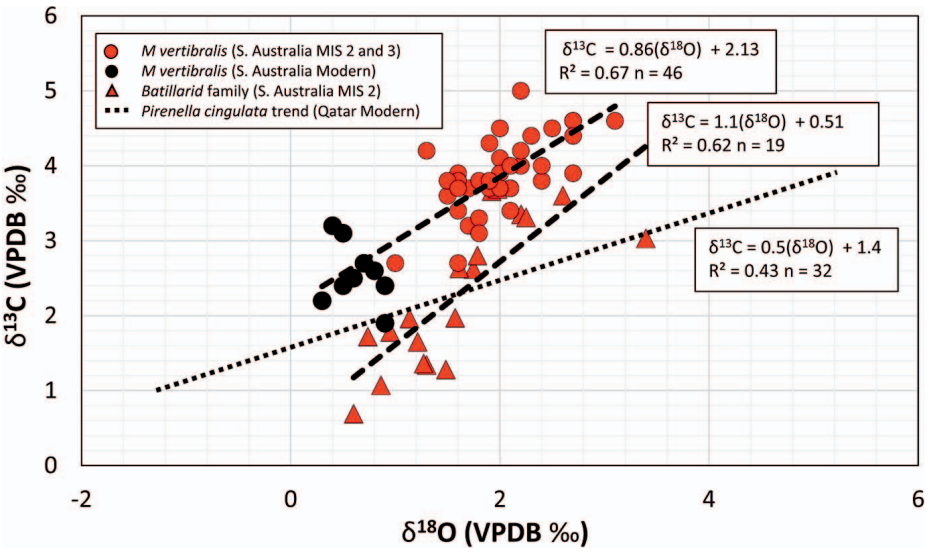

FIG. 14.—Data on $\delta^{18}O$ vs. $\delta^{13}C$ and grouped best-fit trends for *Marginopora vertebralis* taken from the Great Australian Bight, Lincoln, and Lacepede shelves of southern Australia (Rivers et al. 2007, 2009) as well as Cerithidea *Batillaria* data and trend from the same study. Trend of Qatar *Pirenella cingulata* data (data shown on Fig. 10A) also shown.

The $\delta^{18}O$ and $\delta^{13}C$ values of *Pirenella cingulata* gastropods correlate positively, reflecting increasing levels of restriction and evaporation. The $\delta^{18}O$ values of the gastropod shells also strongly correlates with that of the water, with a positive 1:1 slope, indicating that fossil shells of this species may be useful archives for the chemistry of ancient oceans. Measured Sr^{2+} concentration in these gastropods, however, exhibit no correlation with ambient oceanographic measurements at the time of collection, and no systematic difference between collection seasons.

SUPPLEMENTAL MATERIAL

Coastal water chemistry data are available from JSR's Data Archive: https://www.sepm.org/pages.aspx?pageid=229.

ACKNOWLEDGMENTS

This contribution is dedicated to the late T. Kurtis Kyser (the "T" stands for "The"). JMR is grateful for his generous sharing of knowledge and wit. The manuscript was greatly improved by reviews from Stephen Kaczmarek, Luis Gonzalez, Eric Hiatt, and James Bishop. The authors would like to acknowledge the Qatar Civil Aviation Authority, Department of Meteorology, for providing the meteorological data needed. We are grateful to Noel James and Kurtis Kyser at Queen's University, Kingston, Ontario, for chemical analyses of gastropods from the southern Australian margin. Australian samples were collected using CSIRO R.V. Franklin cruises No. FR03/89, FR02/91, FR06/94, FR07/95, FR03/98, and the captain and crew members of each are thanked for their assistance.

REFERENCES

Adams, J.F., and Rhodes, M.L., 1960, Dolomitization by seepage refluxion: American Association of Petroleum Geologists, Bulletin, v. 44, p. 1912–1920.

Aharon, P., Kolodny, Y., and Sass, E., 1977, Recent hot brine dolomitization in the "Solar Lake," Gulf of Elat, Isotopic, chemical, and mineralogical study: The Journal of Geology, v. 85, p. 27–48.

Al-Ansari, E.M., Rowe, G., Abdel-Moati, M., Yiğiterhan, O., and Al-Maslamani, I., 2015, Hypoxia in the central Arabian Gulf Exclusive Economic Zone (EEZ) of Qatar during summer season: Estuarine, Coastal and Shelf Science, v. 159, p. 60–68.

Al Mamoon, A., Joergensen, N.E., Rahman, A., and Qasem, H., 2014, Derivation of new design rainfall in Qatar using L-moment based index frequency approach: International Journal of Sustainable Built Environment, v. 3, p. 111–118.

Al-Saad, H., 2003, Facies analysis, cyclic sedimentation and paleo-environment of the middle Eocene Rus Formation in Qatar and Adjoining Areas: Carbonates and Evaporites, v. 18, p. 41–50.

Alsharhan, A.S., and Kendall, C.G.St.C., 2003, Holocene coastal carbonate and evaporite of the southern Arabian Gulf and their ancient analogues: Earth-Science Reviews, v. 61, p. 191–243.

Annandale, N., and Kemp, S., 1916, Fauna of the Chilka Lake, No. 4, Mollusca, Gastropoda and Lamellibranchiata, with an account of the anatomy of the common Solen: Memoirs of the Indian Museum, v. 5, p, 329–374.

Azam, M.H., Elshorbagy, W., Ichikawa, T., Terasawa, T., and Taguchi, A.K., 2006, 3D model application to study residual flow in the Arabian Gulf: Journal of Waterway, Port, Coastal, and Ocean Engineering, v. 132, p. 388–400.

Billeaud, I., Caline, B., Livas, B., Tessier, B., Davaud, E.J., Frebourg, G., Hasler, C.A., and Laurier, D., 2014, The carbonate–evaporite lagoon of Al Dakhirah (Qatar): an example of a modern depositional model controlled by longshore transport, *in* Martini, I.P., and Wanless, H.R., eds., Sedimentary Coastal Zones from High to Low Latitudes: Similarities and Differences: Geological Society of London, Special Publication 388, p. 561–287.

Bontognali, T.R.R., Vasconcelos, C., Warthmann, R.J., Bernasconi, S.M., Dupraz, C., Strohmenger, C.J., and McKenzie, J.A., 2010, Dolomite formation within microbial mats in the coastal sabkha of Abu Dhabi (United Arab Emirates): Sedimentology, v. 57, p. 824–844.

Brauchli, M., McKenzie, J.A., Strohmenger, C.J., Sadooni, F., Vasconcelos, C., and Bontognali, T., 2016, The importance of microbial mats for dolomite formation in the Dohat Faishakh sabkha, Qatar: Carbonates and Evaporites, v. 31, p. 339.

Butler, G.P., Harris, P.M., and Kendall, C.G.St.C., 1982, Recent evaporites from the Abu Dhabi coastal flats, *in* Robertson, C., ed., Depositional and Diagenetic Spectra of Evaporites: SEPM, Core Workshop 3A, Calgary, p. 33–64.

Craig, H., 1961, Standard for reporting concentrations of deuterium and oxygen 18 in natural water: Science, v. 133, p. 1833.

Craig, H., and Gordon, L.I., 1965, Deuterium and oxygen 18 variations in the ocean and the marine atmosphere: Spokto Conference on Stable Isotopes in Oceanographic Studies and Paleotemperatures, Laboratorio di Geologia Nucleate, Italy, Proceedings.

Dettman, D.L., Reische, A.K., and Lohmann, KC., 1999, Controls on the stable isotope composition of seasonal growth bands in aragonitic freshwater bivalves (Unionidae): Geochimica et Cosmochimica Acta, v. 63, p. 1049–1057.

Dufour, V., Pierre, C., and Rancher, J., 1998, Stable isotopes in fish otoliths discriminate between lagoonal and oceanic residents of Taiaro Atoll (Tuamotu Archipelago, French Polynesia): Coral Reefs, v. 17, p. 23–28.

Elhakeem, A., Elshorbagy, W., and Bleninger, T., 2015, Long-term hydrodynamic modeling of the Arabian Gulf: Marine Pollution Bulletin, v. 94, p. 19–36.

Elshorbagy, W., Azam, M.H., Nakata, K., and Terasawa, T., 2007, Temperature–salinity field of the shallow shelf of the southern Arabian Gulf: Far East Journal of Ocean Research, v. 1, p. 99–126.

Engel, M., and Brückner, H., 2014, The South Qatar Survey Project (SQSP): preliminary findings on Holocene coastal changes and geoarchaeological archives: Zeitschrift für Orient-Archäologie, v. 7, p. 290–301.

Erftemeijer, P., de Graaff, R., and Boot, G., 2004, Site selection for artificial reefs in Bahrain (Arabian Gulf) based on GIS technology and hydrodynamic modelling: Journal of Marine Science and Environment, v. 2, p. 29–38.

Esri, DigitalGlobe, GeoEye, i-cubed, USDA FSA, USGS, AEX, Getmapping, Aerogrid, IGN, IGP swisstopo, and the GIS User Community.

Evamy, B.D., 1973, The precipitation of aragonite and its alteration to calcite on the Trucial coast of the Persian Gulf *in* Purser, B.H., ed., The Persian Gulf: Holocene Carbonate Sedimentation and Diagenesis in a Shallow Epicontinental Sea: New York, Springer, p. 211–232.

Evans, G., Schmidt, V., Bush, P., and Nelson, H., 1969, Stratigraphy and geologic history of the sabkha, Abu Dhabi, Persian Gulf: Sedimentology, v. 12, p. 145–159.

Gischler, E., and Lomando, A.J., 1997, Holocene cemented beach deposits in Belize: Sedimentary Geology, v. 110, p. 277–297.

Gonfiantini, R., and Fontes, J.C., 1963, Oxygen isotopic fractionation in the water of crystallization of gypsum: Nature, v. 200, p. 644–646.

Grossman, E.L., and Ku, T.L., 1986, Oxygen and carbon isotope fractionation in biogenic aragonite: temperature effects: Chemical Geology, v. 59, p. 59–74.

Hardie, A., and Eugster, P., 1970, The evolution of closed-basin brines: Special Paper Mineralogical Society of America, Special Paper 3, p. 273–390.

Hofmann, G.E., Smith, J.E., Johnson, K.S., Send, U., Levin, L.A., Micheli, F., Paytan, A., Price, N.N., Peterson, B., Takeshita, Y., Matson, P.G., Crook, E.D., Kroeker, K.J., Gambi, M.C., Rivest, E.B., Frieder, C.A., Yu, P.C., and Martz, T.R., 2011, High-frequency dynamics of ocean pH: a multi-ecosystem comparison: PLOS One, v. 6, p. 1–11.

Holser, W., 1979, Trace elements and isotopes in evaporites, *in* Burns, R.G., ed., Marine Minerals: Mineralogical Society of America, Reviews in Mineralogy, v. 6, p. 295–346.

Hsu, K.J., and Schneider, J., 1973, Progress report on dolomitization-hydrology of Abu Dhabi sabkhas, Arabian Gulf, *in* Purser, B.H., ed., The Persian Gulf: New York, Springer, p. 409–422.

Hsu, K.J., and Siegenthaler, C., 1969, Preliminary experiments on hydrodynamic movement induced by evaporation and their bearing on the dolomite problem: Sedimentology, v. 12, p. 11–25.

IAEA (International Atomic Energy Agency, Vienna), 1992, Statistical Treatment of Data on Environmental Isotopes in Precipitation, Technical Reports Series, n. 331.

Illing, L.V., Wells A.J., and Taylor, J.C.M., 1965, Penecontemporary dolomite in the Persian Gulf, *in* Pray, L.C., and Murray, L.C., eds., Dolomitization and Limestone Diagenesis: SEPM, Special Publication 13, p. 89–111.

Illing, L.V., and Taylor, J.C.M., 1993, Penecontemporaneous dolomitization in Sabkha Faishakh, Qatar: evidence from changes in the chemistry of the interstitial brines: Journal of Sedimentary Petrology, v. 63, p. 1042–1048.

Jutting B., and Van, W.S.S., 1956, Systematic studies on the non-marine Mollusca of the Indo-Australian archipelago: Treubia, v. 23, p. 259–477.

Kaczmarek, S.E., and Thornton, B.P., 2017, The effect of temperature on stoichiometry, cation ordering, and reaction rate in high-temperature dolomitization experiments: Chemical Geology, v. 468, p. 32–41.

Kaczmarek, S.E., Gregg, J.M., Bish, D., Machel, H., and Fouke, B., 2017, Dolomite, very-high magnesium calcite, and microbes: implications for the microbial model of dolomitization, *in* MacNeil, A., Lonnee, J., and Wood, R., eds., Characterization and Modeling of Carbonates, Mountjoy Symposium I: SEPM, Special Publication 109, p. 7–20.

Kampf, J., and Sadrinasab, M., 2006, The circulation of the Persian Gulf: a numerical Study: Ocean Science, v. 2, p. 27–41.

Kinsman, D.J.J., 1964, The recent carbonate sediments near Halat el Bahrani, Trucial Coast, Persian Gulf, *in* van Straaten, L.M.J.U., ed., Deltaic and Shallow Marine Deposits: Amsterdam, Elsevier, Developments in Sedimentology 1, p. 185–192.

Knauth, L.P., and Beeunas, M.A., 1986, Isotope geochemistry of fluid inclusions in Permian halite with implications for the isotopic history of ocean water and the origin of saline formation waters: Geochimica et Cosmochimica Acta, v. 50, p. 419–433.

Krumgalz, B.S., 2001, Application of the Pitzer ion interaction model to natural hypersaline brines: Journal of Molecular Liquids, v. 91, p. 3–19.

Lazar, B., and Erez, J., 1992, Carbon geochemistry of marine derived brines: I. ^{13}C depletions due to intense photosynthesis: Geochimica et Cosmochimica Acta, v. 56, p. 335–345.

Lazar, B., Starinsky, A., Katz, A., and Sass, E., 1983, The carbonate system in hypersaline solutions: alkalinity and $CaCO_3$ solubility of evaporated seawater: Limnology and Oceanography, v. 28, p. 978–986.

Lloyd, R.M., 1966, Oxygen isotope enrichment of sea water by evaporation: Geochimica et Cosmochimica Acta, v. 30, p. 801–814.

Loreau, J., and Purser, B.H., 1973, Distribution and ultrastructure of Holocene ooids in the Persian Gulf *in* Purser, B.H., ed., The Persian Gulf: Holocene Carbonate Sedimentation and Diagenesis in a Shallow Epicontinental Sea: New York, Springer, p. 233–289.

Major, R.P., Lloyd, R.M., and Lucia, F.J., 1992, Oxygen isotope composition of Holocene dolomite formed in a humid hypersaline setting: Geology, v. 20, p. 586–588.

Markham, A.E., and Kobe, K.A., 1941, The solubility of carbon dioxide and nitrous oxide in aquesalt solutions, American Chemical Society, Journal, v. 63, p. 449–454.

McCaffrey, M.A., Lazar, B., and Holland, H.D., 1987, The evaporation path of seawater and the coprecipitation of Br(–) and K(+) with halite: Journal of Sedimentary Petrology, v. 57, p. 928–937.

Morse, J.W., and Mackenzie, F.T., 1990, Geochemistry of Sedimentary Carbonates: Amsterdam, Elsevier, 707 p.

Ozawa, T., Köhler, F., Reid, D.G., and Glaubrecht, M., 2009, Tethyan relicts on continental coastlines of the northwestern Pacific Ocean and Australasia: molecular phylogeny and fossil record of batillariid gastropods (Caenogastropoda, Cerithioidea): Zoologica Scripta, v. 38, p. 503–525.

Parkhurst, D.L., and Appelo, C.A.J., 2013, Description of input and examples for PHREEQC version 3. A computer program for speciation, batch-reaction, one-dimensional transport, and inverse geochemical calculations: U.S. Geological Survey, Techniques and Methods, Book 6, 497 p.

Paulo, C., and Dittrich, M., 2013, 2D Raman spectroscopy study of dolomite and cyanobacterial extracellular polymeric substances from Khor Al-Adaid sabkha (Qatar): Journal of Raman Spectroscopy, v. 44, p. 1563–1569.

Petrash, D.A., Bialik, O.M., Bontognali, T.R.R., Vasconcelos, C., Roberts, J.A., McKenzie, J.A., and Konhauser, K.O., 2017, Microbially catalyzed dolomite formation: From near-surface to burial: Earth-Science Reviews, v. 171, p. 558–582.

Plummer, L.N., Parkhurst, D.L., Fleming, G.W., and Dunkle, S.A., 1988, A Computer Program Incorporating Pitzer's Equations for Calculation of Geochemical Reactions in Brines: U.S. Geological Survey, Water-Resources Investigations, Report 88-4153, p. 310.

Purkis, S., Rivers, J., Yousif, R., Warren, C., and Strohmenger, C., 2017, Complex interplay between depositional and petrophysical environments on a Holocene tidal flat (Al Ruwais, Qatar): Sedimentology, p. 1–30.

Purser, B.H., 1973, The Persian Gulf: Holocene Carbonate Sedimentation and Diagenesis in a Shallow Epicontinental Sea: New York, Springer, 471 p.

Purser, B.H., and Evans, G., 1973, Regional sedimentation along the Trucial Coast, SE Persian Gulf, *in* Purser, B.H., ed., The Persian Gulf: Holocene Carbonate Sedimentation and Diagenesis in a Shallow Epicontinental Sea: New York, Springer, p. 211–232.

Purser, B.H., and Loreau, J.P., 1973, Aragonitic, supratidal encrustations on the Trucial Coast, Persian Gulf, *in* Purser, B.H., ed., The Persian Gulf: Holocene Carbonate Sedimentation and Diagenesis in a Shallow Epicontinental Sea: New York, Springer, p. 343–376.

Purser, B.H., and Seibold, E., 1973, The principal environmental factors influencing Holocene sedimentation and diagenesis in the Persian Gulf, *in* Purser, B.H., ed., The Persian Gulf: Holocene Carbonate Sedimentation and Diagenesis in a Shallow Epicontinental Sea: New York, Springer, p. 1–10.

Rao, Y.P., and Rao, D.G.V.P., 1983, Effect of temperature on aquatic and aerial oxygen consumption of *Cerithidea* (Cerithideopsilla) *cingulata* (Gmelin) and *Cerithium coralium* Kiener (Mollusca Gastropoda): Italian Journal of Zoology, v. 17, p. 113–119.

Read, J.F., 1982, Carbonate platforms of passive (extensional) continental margins: types, characteristics, and evolution: Tectonophysics, v. 81, p. 195–212

Reid, D., and Ozawa, T., 2016, The genus Pirenella Gray, 1847 (*Cerithideopsilla thiele* 1929) (Gastropoda: Potamididae) in the Indo-West Pacific region and Mediterranean Sea: Zootaxa, v. 4076, p. 1–91.

Rezaei-Latifi, A., 2016, Variability of Fresnel surface emissivity of Persian Gulf water in a nadir-viewing direction at C- band: Journal of Radiation Research and Applied Sciences, v. 9, p. 131–138.

Rivers, J.M., James, N.P., and Kyser, T.K., 2007, Genesis of palimpsest cool-water carbonate sediment on the southern Australian margin: Journal of Sedimentary Research, v. 77, p. 480–494.

Rivers, J.M., Kyser, T.K., and James, N.P., 2009, Isotopic composition of a large benthic foraminifer: evidence for hypersaline environments across the Great Australian Bight during the Late Pleistocene: Sedimentary Geology, v. 213, p. 113–120.

Rivers, J.M., Kyser, T.K., and James, N.P., 2012, Salinity reflux and dolomitization of southern Australian slope sediments: the importance of low carbonate saturation levels: Sedimentology, v. 59, p. 445–465.

Sadooni, F.N., Howari, F., and El-Saiy, A., 2010, Microbial dolomites from carbonate–evaporite sediments of the coastal sabkha of Abu Dhabi and their exploration implications: Journal of Petroleum Geology, v. 33, p. 289–298.

Sadrinasab, M., and Kenarkohi, K., 2009, Three-dimensional numerical modelling study of sound speed in the Persian Gulf: Asian Journal of Applied Sciences, v. 2, p. 232–239.

Seltrust Engineering Limited, 1980, Qatar Geological Map and Explanatory Booklet, Doha, Qatar: London, Industrial Development and Technical Centre.

Shen, Z., Liu, Y., Brown, P.E., Szlufarska, I., and Xu, H., 2014, Modeling the effect of dissolved hydrogen sulfide on Mg^{2+}-water complex on dolomite {104} surfaces: Journal of Physical Chemistry C, v. 118, p. 15,716–15,722.

Shinn, E.A., 1969, Submarine lithification of Holocene carbonate sediments in the Persian Gulf: Sedimentology, v. 12, p. 109–144.

Shinn, E.A., 1973, Sedimentary accretion along the leeward, SE coast of Qatar Peninsula, Persian Gulf, *in* Purser, B.H., ed., The Persian Gulf: Holocene Carbonate Sedimentation and Diagenesis in a Shallow Epicontinental Sea: New York, Springer, p. 199–209.

Smith, S.V., and Veeh, H.H., 1989, Mass balance of biogeochemically active materials (C, N, P) in a hypersaline gulf: Estuarine, Coastal and Shelf Science, v. 29, p. 195–215.

Smith, S.V., Buddemeier, R.W., Redalje, R.C., and Houck, J.E., 1979, Strontium–calcium thermometry in coral skeletons: Science, v. 204, p. 404–406.

Spero, H.J., Bijma, J., Lea, D.W., and Bemis, B.E., 1997, Effect of seawater carbonate concentration on foraminiferal carbon and oxygen isotopes: Nature, v. 390, p. 497–500.

Sreenivasan, P.V., 1985, Studies on the Potamidid snail, *Cerithidea* (Cerithideopsilla) *cingulata* (Mollusca, Mesogastropoda): Centre of Advanced Study in Marine Biology, Annamalai University.

Sreenivasan, P.V., and Natatajan, R., 1991, Potamidid snails of Vellar-Coleroon Estuarine Area, Southeast Coast of India: Marine Biological Association of India, Journal, v. 33, p. 385–395.

Stern, R.J., and Johnson P., 2010, Continental lithosphere of the Arabian plate; a geologic, petrologic, and geophysical synthesis: Earth-Science Reviews, v. 101, p. 29–67.

Sun, S.Q., 1992, Skeletal aragonite dissolution from hypersaline sea water: a hypothesis: Sedimentary Geology, v. 77, p. 249–257.

Vahrenkamp, V.C., and Swart, P.K., 1990, New distribution coefficient for the incorporation of strontium into dolomite and its implications for the formation of ancient dolomites: Geology, v. 18, p. 387–391.

Veizer, J., Holser, W.T., and Wilgus, C.K., 1980, Correlation of $^{13}C/^{12}C$ and $^{34}S/^{32}S$ secular variations: Geochimica et Cosmochimica Acta, v. 44, p. 579–587.

Veizer, J., Bruckschen, P., Pawellek, F., Diener, A., Podlaha, O.G., Jasper, T., Korte, C., Carden, G.A.F., Strauss, H., Azmy, K., and Ala, D., 1997, Oxygen isotope evolution of Phanerozoic seawater: Paleogeography, Paleoclimatology, Paleoecology, v. 132, p. 159–172.

Veizer, J., Godderis, Y., and Francois, L.M., 2000, Evidence for decoupling of atmospheric CO_2 and global climate during the Phanerozoic Eon: Nature, v. 8, p. 698–701.

Wagner, C.W., and Van der Togt, C., 1973, Holocene sediment types and their distribution in the Southern Persian Gulf *in* Purser, B.H., ed., The Persian Gulf: Holocene Carbonate Sedimentation and Diagenesis in a Shallow Epicontinental Sea: New York, Springer, p. 123–155.

Warren, J., 2000, Dolomite: occurrence, evolution and economically important associations: Earth-Science Reviews, v. 52, p. 1–81.

Warren, J.K., 2006, Evaporites; Sediments, Resources, and Hydrocarbons: New York, Springer, 1035 p.

Warren, J.K., 2016, Evaporites: A Geological Compendium, Second Edition: New York, Springer, 1813 p.

Wilkinson, B.H., and Drummond, C.N., 2004, Facies mosaics across the Persian Gulf and around Antigua: stochastic and deterministic products of shallow water sediment accumulation: Journal of Sedimentary Research, v. 74, p. 513–526.

Zeebe, R.E., 1999, An explanation of the effect of seawater carbonate concentration on foraminiferal oxygen isotopes: Geochimica et Cosmochimica Acta v. 63, p. 2001–2007.

Received 8 February 2018; accepted 31 December 2018.